MBoC | ARTICLE

Differential reliance of CTD-nuclear envelope phosphatase 1 on its regulatory subunit in ER lipid synthesis and storage

Jake W. Carrasquillo Rodríguez[a], Onyedikachi Uche[a], Shujuan Gao[b], Shoken Lee[a], Michael V. Airola[b], and Shirin Bahmanyar[a,*]

[a]Department of Molecular, Cellular and Developmental Biology, Yale University, New Haven, CT 06511; [b]Department of Biochemistry and Cell Biology, Stony Brook University, Stony Brook NY 11794

ABSTRACT **Lipin 1 is an ER enzyme that produces diacylglycerol, the lipid intermediate that feeds into the synthesis of glycerophospholipids for membrane expansion or triacylglycerol for storage into lipid droplets. CTD-Nuclear Envelope Phosphatase 1 (CTDNEP1) regulates lipin 1 to restrict ER membrane synthesis, but a role for CTDNEP1 in lipid storage in mammalian cells is not known. Furthermore, how NEP1R1, the regulatory subunit of CTDNEP1, contributes to these functions in mammalian cells is not fully understood. Here, we show that CTDNEP1 is reliant on NEP1R1 for its stability and function in limiting ER expansion. CTDNEP1 contains an amphipathic helix at its N-terminus that targets to the ER, nuclear envelope and lipid droplets. We identify key residues at the binding interface of CTDNEP1 and NEP1R1 and show that they facilitate complex formation in vivo and in vitro. We demonstrate that NEP1R1 binding to CTDNEP1 shields CTDNEP1 from proteasomal degradation to regulate lipin 1 and restrict ER size. Unexpectedly, NEP1R1 was not required for CTDNEP1's role in restricting lipid droplet biogenesis. Thus, the reliance of CTDNEP1 function on NEP1R1 depends on cellular demands for membrane production versus lipid storage. Together, our work provides a framework into understanding how the ER regulates lipid synthesis under different metabolic conditions.**

SIGNIFICANCE STATEMENT

- The endoplasmic reticulum is the site of membrane synthesis and lipid storage. The phosphatidic acid phosphatase lipin 1 produces the lipid precursor for both reactions. Human CTDNEP1 regulates lipin 1 and has a regulatory subunit called NEP1R1. The role of the CTDNEP1-NEP1R1 complex in regulation of lipin 1 for ER membrane synthesis and lipid storage is not known.
- Structure-function analysis, in silico modeling and biochemical approaches show that NEP1R1 stabilizes CTDNEP1 to restrict ER membrane synthesis, but this interaction is not essential for CTDNEP1's role in lipid storage.
- Thus, differential regulation of CTDNEP1 in ER membrane synthesis and lipid storage ensures lipid homeostasis.

Monitoring Editor
Guillaume Thibault
Nanyang Technological University

Received: Oct 10, 2023
Revised: May 6, 2024
Accepted: May 17, 2024

New Hypothesis

This article was published online ahead of print in MBoC in Press (http://www.molbiolcell.org/cgi/doi/10.1091/mbc.E23-09-0382) on May 22, 2024.

Contributions: J.W.C.R. and S.B. conceived the project. J.W.CR. performed most of the experiments and data analysis. O.U. performed experiments for ER expansion, nuclear solidity and lipin 1 localization in the CTDNEP1-HA stable variants. S.G. performed experiments for protein purification, size exclusion chromatography and p-NPP analysis of CTDNEP1/NEP1R1 in-vitro with M.V.A. supervision. S.L. performed experiments in endogenously tagged CTDNEP1^mAID-HA cells for NEP1R1 RNAi, wrote the IJ Macro and Python scripts for LD analysis. J.W.C.R., M.V.A., and S.B. wrote the manuscript with input from other authors. S.B. and M.V.A supervised the project.

*Address correspondence to: Shirin Bahmanyar, (shirin.bahmanyar@yale.edu).

Abbreviations used: AH, amphipathic helix; CTDNEP1, CTD nuclear envelope phosphatase 1; DAG, diacylglycerol; ER, endoplasmic reticulum; LD, lipid droplet; mAID, mini-Auxin inducible degron; NEP1R1, nuclear envelope phosphatase-regulatory subunit 1; PA, phosphatidic acid; TAG, triacylglycerol.

INTRODUCTION

The endoplasmic reticulum (ER) is the largest organelle in cells and is made up of distinct structural and functional domains that include the nuclear envelope (Baumann and Walz, 2001; Friedman *et al.*, 2011). Much of the protein machinery in the ER functions in the synthesis, processing and trafficking of secreted proteins. Protein quality control mechanisms recognize misfolded proteins and target them for degradation by the ER-associated degradation pathway (Mehrtash and Hochstrasser, 2018; Christianson *et al.*, 2023). The AAA$^+$-ATPase p97 cooperates with the proteasome to extract membrane proteins for their subsequent degradation (Meyer *et al.*, 2012).

The ER is also the site of de novo synthesis for most membrane and storage lipids (Fagone and Jackowski, 2009). Enzymes embedded or peripherally associated with the surface of the ER carry out a series of sequential reactions to produce the major membrane phospholipids (e.g., phosphatidylcholine and phosphatidylethanolamine) from diacylglycerol (DAG) and a more minor pool of lipid (e.g., phosphatidylinositol) from phosphatidic acid (PA). Activated fatty acids combine with lysophosphatidic acid (LPA) to produce PA, which is dephosphorylated to generate DAG. DAG can also be converted to triglycerides (TAG; Walther and Farese, 2012). TAGs accumulate in specialized storage organelles called lipid droplets (LDs), which are derived from the ER and protect cells from buildup of excess fatty acids that can negatively affect membrane function (Coleman *et al.*, 2000; Olzmann and Carvalho, 2019). Feedback mechanisms maintain ER lipid homeostasis by sensing and responding to biochemical fluxes in lipid levels (Goldstein *et al.*, 2006; Olzmann and Carvalho, 2019). These feedback mechanisms control the quantity of lipid enzymes through the ER-associated degradation machinery as well as regulation of transcriptional networks (Stevenson *et al.*, 2016).

As the major supplier of membrane lipids for organelles, the ER must maintain its overall structure and size. How the production of membranes is regulated to control ER size and dynamics in animal cells is not fully understood. Addressing this question requires that we understand the upstream mechanisms that control whether DAG is converted into membrane phospholipids to expand the ER or into TAG for storage into LDs.

Here, we focus on the nuclear envelope-associated protein phosphatase CTD-nuclear envelope phosphatase 1 (CTDNEP1, formerly known as Dullard; Nem1 in *Saccharomyces cerevisiae*, CNEP-1 in *Caenorhabditis elegans*) because of its conserved role from yeast to humans in restricting ER membrane production and thus size (Siniossoglou *et al.*, 1998; Santos-Rosa *et al.*, 2005; O'Hara *et al.*, 2006; Kim *et al.*, 2007; Han *et al.*, 2012; Bahmanyar *et al.*, 2014; Jacquemyn *et al.*, 2021; Merta *et al.*, 2021). CTDNEP1 is the master regulator of the PA phosphatase lipin 1, the main ER enzyme that coverts PA into DAG (Siniossoglou *et al.*, 1998; Han *et al.*, 2012; Merta *et al.*, 2021; Lee *et al.*, 2023). CTDNEP1 is a member of the C-Terminal Domain-family of Ser/Thr phosphatases that is defined by a signature DXDX(T/V) motif in the catalytic domain (Seifried *et al.*, 2013; Figure 1A). CTD-family phosphatases evolved independently from PP1/PP2 alkaline phosphatases or tyrosine phosphatases and appear to have exquisite specificity for their substrates; however, little is known about how different members of the CTD-family of protein phosphatases recognize their distinct substrates (Seifried *et al.*, 2013).

CTDNEP1 maintains a stable, dephosphorylated pool of lipin 1 by opposing stimulatory signals from the mTORC1 nutrient sensing pathway (Merta *et al.*, 2021; Lee *et al.*, 2023). In addition to being the major ER enzyme that converts PA to DAG, a pool of dephosphorylated lipin 1 is nuclear-localized and has a role in restricting the transcription of fatty acid synthesis genes (Peterson *et al.*, 2011; Merta *et al.*, 2021). Reducing lipin 1 levels shrinks the ER because lowering DAG production limits membrane synthesis (Merta *et al.*, 2021). In contrast, deletion of CTDNEP1 expanded the ER because loss of dephosphorylated lipin 1 increased de novo synthesis of fatty acids (Merta *et al.*, 2021). Interestingly, CTDNEP1 is also involved in stabilization of the resident NE protein, Sun2 (Krshnan *et al.*, 2022; Lee *et al.*, 2023) through its role in regulation of lipid metabolism (Lee *et al.*, 2023).

Important work in budding yeast elucidated mechanisms that regulate the conserved lipin activation pathway to control ER lipid homeostasis (Santos-Rosa *et al.*, 2005; Han *et al.*, 2006; O'Hara *et al.*, 2006; Han *et al.*, 2008; Karanasios *et al.*, 2013; Park *et al.*, 2017; Kwiatek and Carman, 2020; Kwiatek *et al.*, 2020; Mirheydari *et al.*, 2020; Jog *et al.*, 2023). However, metazoans use DAG as a precursor for both the production and storage of lipids (Figure 1A), whereas fungi utilize PA for the synthesis of major membrane phospholipids (Coleman and Lee, 2004). In addition to these differences, emerging evidence for a tumor suppressor function of human CTDNEP1 motivates an in-depth analysis of its regulation in mammalian cells.

We show that CTDNEP1 evolved an N-terminal amphipathic helix (AH) required for its targeting to the ER/nuclear envelope and the surface of LDs. The integral membrane binding partner, Nuclear Envelope Phosphatase 1-Regulatory subunit 1 (NEP1R1; Figure 1A), stabilized CTDNEP1 protein, preventing membrane extraction by the AAA$^+$-ATPase p97 and degradation by the proteasome. Both peripheral membrane binding and stabilization of CTDNEP1 by NEP1R1 were required to promote lipin 1 dephosphorylation and restrict ER membrane production under basal conditions. In cells fed with excess fatty acids, CTDNEP1 phosphatase activity limited lipid droplet formation; however, the interaction between CTDNEP1 and NEP1R1 was no longer relevant to CTDNEP1's localization to LDs nor its role in limiting their biogenesis. Our work suggests that metabolic reprogramming from membrane synthesis to lipid storage may rewire the requirement for CTDNEP1 complex formation with NEP1R1 to locally control lipid droplet biogenesis. Our findings underscore the role of CTDNEP1 as a major regulator of lipid synthesis in animal cells and highlight the importance of gaining a mechanistic understanding for its regulation, especially in light of its critical role as a potential tumor suppressor.

RESULTS

Different mechanisms target and stabilize CTDNEP1 at ER and nuclear membranes

Our recent work shows that NEP1R1 directly binds and increases the activity of CTDNEP1 in vitro (Gao *et al.*, 2024). In line with this, prior work in human cells showed that transient coexpression of NEP1R1 and CTDNEP1 under control of constitutive promoters increased the protein levels of exogenous CTDNEP1 and promoted lipin dephosphorylation (Han *et al.*, 2012). However, the effect of NEP1R1 on the protein abundance, localization and activity of endogenous CTDNEP1 in cells had not been tested.

We utilized our CRISPR-Cas9 gene edited cell lines with either EGFP or HA inserted at the endogenous locus of CTDNEP1 (CTDNEP1^EGFP in U2OS cells and CTDNEP1^mAID-HA in DLD-1 cells, Lee *et al.*, 2023) to test how NEP1R1 impacts the steady state localization and protein levels of endogenous CTDNEP1. CTDNEP1^EGFP localized in a punctate pattern at the NE, as reported (Lee *et al.*, 2023), and was colocalized with an ER marker in the perinuclear region and faintly to ER tubules in the cell periphery

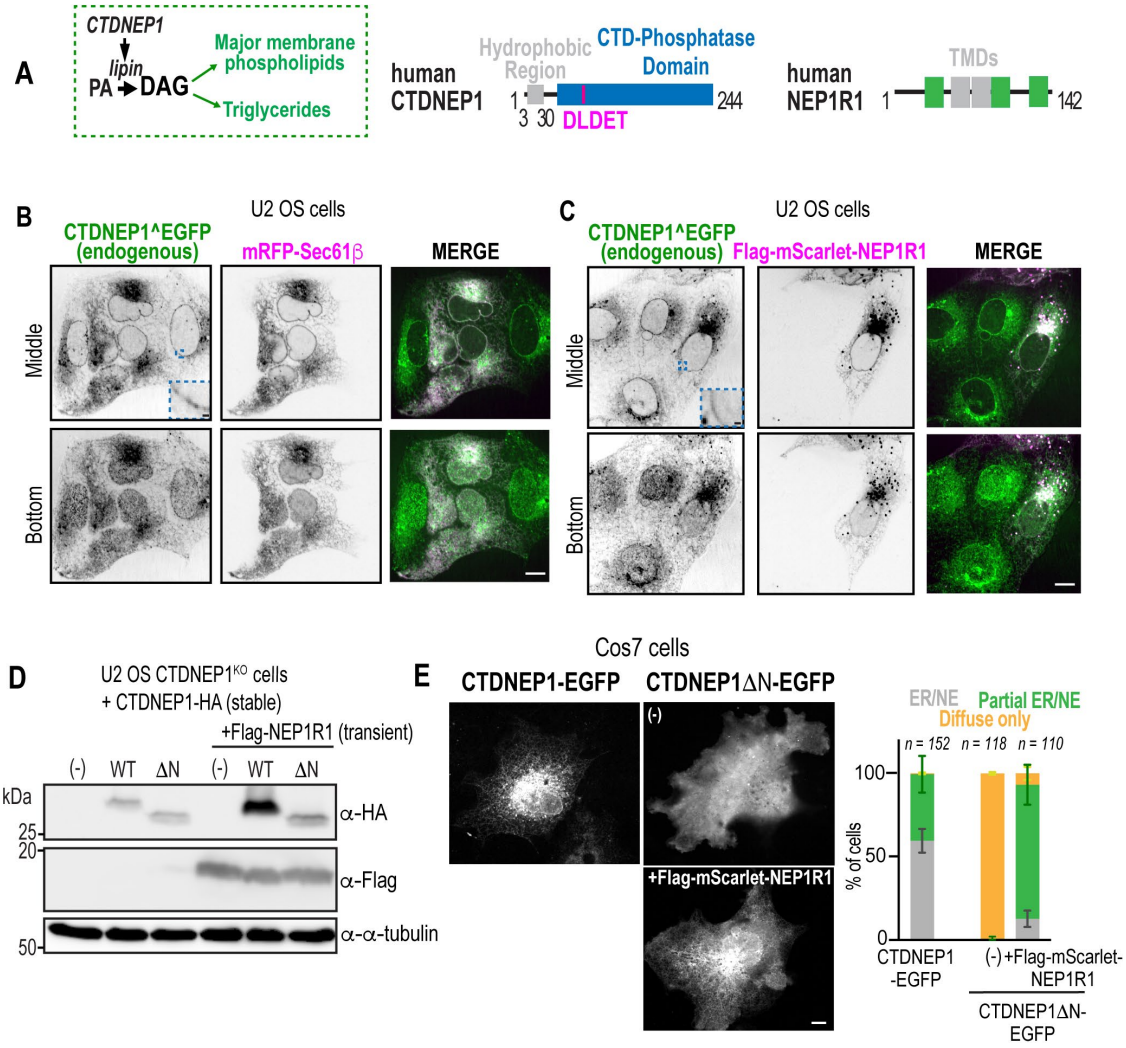

FIGURE 1. ER and nuclear envelope targeting and stabilization of CTDNEP1 depends on its N-terminal hydrophobic region. (A) Left: Schematic representation of PA to DAG conversion for de novo lipid synthesis. Right: Schematic representation of CTDNEP1 and NEP1R1 protein domains. (B) Representative spinning disk confocal images of CTDNEP1^EGFP and mRFP-Sec61β in living cells. Inset shows nuclear envelope localization of CTDNEP1^EGFP. Scale bar, 10 μm; Scale bar inset, 1 μm; *N* = 2 independent experiments. (C) Representative spinning disk confocal images of CTDNEP1^EGFP in cells transfected with Flag-mScarlet-NEP1R1. Inset shows nuclear envelope localization of CTDNEP1^EGFP. Scale bar, 10 μm; Scale bar inset, 1 μm; *N* = 2 independent experiments. (D) Immunoblot of whole cell lysates from CTDNEP1-deleted cells cotransfected with CTDNEP1-HA variants and Flag-NEP1R1. *N* = 3 independent experiments. (E) Left: Representative spinning disk confocal images of indicated CTDNEP1-EGFP variants transiently transfected in living Cos-7 cells. Scale bar, 10 μm. Right: Plot, blind quantification of CTDNEP1-EGFP localization under conditions on the left. Mean ± SD shown, *n* = individual cells counted. *N* = 3 independent experiments.

(Figure 1B). Punctate CTDNEP1^EGFP structures were also present and these often colocalized with the lysosomal marker Lamp1-mScarlet (Supplemental Figure S1A). Transient NEP1R1 overexpression in a subset of cells resulted in an ~30% increase in endogenous CTDNEP1^EGFP protein levels, as observed by immunoblot (Supplemental Figure S1B). Single cell analysis revealed that CTDNEP1^EGFP was more uniform throughout the ER and NE in NEP1R1 overexpressing cells and there was an increased abundance of puncta containing CTDNEP1 and NEP1R1 that resemble lysosomal structures (Figure 1C). RNAi-depletion of NEP1R1 uniformly reduced ER and NE-localized CTDNEP1^EGFP (Supplemental Figure S1C), consistent with the strong reduction in endogenous CTDNEP1 protein, but not mRNA, levels (Supplemental Figure S1, D and E). Together, these results indicate that NEP1R1 broadly affects protein levels of ER and nuclear envelope-associated endogenous CTDNEP1.

Work in budding yeast showed that the membrane association of Nem1 (CTDNEP1 in mammals) is mediated by both binding to Spo7 (NEP1R1 in mammals) through its C-terminal catalytic domain and through its N-terminal hydrophobic region (Siniossoglou *et al.*, 1998; Supplemental Figure S1F). To test whether the catalytic domain of CTDNEP1 is sufficient for targeting and stabilization of CTDNEP1 by NEP1R1, we transiently coexpressed NEP1R1 with full length CTDNEP1 or with the N-terminal hydrophobic region deleted (WT and ΔN, deletion of residues 3–30; see Figure 1A). Transient NEP1R1 and CTDNEP1 coexpression substantially increased the protein levels of WT CTDNEP1, as expected (Han *et al.*, 2012), but only slightly increased the protein levels of CTDNEP1ΔN (Figure 1D). Furthermore,

overexpressed CTDNEP1-EGFP uniformly localized to the ER and NE (Figure 1E) and was mostly present in a detergent-soluble pool (Supplemental Figure S1G), whereas CTDNEP1ΔN was diffusely-localized and this pool was likely nonmembrane bound because it was soluble even in the absence of detergent (Figure 1E; Supplemental Figure S1G). The ER and NE localization of CTDNEP1ΔN was only partially restored in cells transiently coexpressing NEP1R1 (Figure 1E). Thus, the C-terminal phosphatase domain of CTDNEP1 is not sufficient for its recruitment to the ER and NE nor its stable association with NEP1R1 in mammalian cells.

The N-terminus of CTDNEP1 encodes an amphipathic helix that is sufficient for targeting the ER, nuclear envelope and the surface of LDs

The hydrophobic region in Nem1 is 39 amino acids, and prior reports have suggested that it is a double pass transmembrane domain (Siniossoglou *et al.*, 1998; Supplemental Figure S1F). Human CTDNEP1 contains a shorter hydrophobic helix of 28 amino acids (residues 3–30; Figure 1A) that had been predicted to encode for a membrane spanning helix (Kim *et al.*, 2007); however, with this orientation the C-terminal phosphatase domain would face the ER lumen (Supplemental Figure S1H). Our in-silico Heliquest analysis and AlphaFold complex structure prediction suggested that the N-terminal residues 3–30 of CTDNEP1 encode for a membrane-associated amphipathic helix (AH) (Supplemental Figure S1, I and J). Amphipathic helices bind at the polar-nonpolar interface of membranes (Gautier *et al.*, 2008; Drin and Antonny, 2010; Gimenez-Andres *et al.*, 2018), which would fit with the expected cytoplasmic/nucleoplasmic facing orientation of the phosphatase domain of CTDNEP1 (Supplemental Figure S1I; Lee *et al.*, 2023). Multiple sequences alignments did not reveal high amino acid identity of the N-terminal region of CTDNEP1 across metazoans tested, however Heliquest predictions showed that the amphiphilicity of CTDNEP1's N-terminus is conserved (Supplemental Figure S2, A and B).

Several lines of evidence further corroborated that the N-terminus of CTDNEP1 encodes for an AH. CTDNEP1 bound to liposome a in-vitro via its N-terminus (Gao *et al.*, 2024). The N-terminal residues 3–30 fused to EGFP alone (hereafter AH-EGFP) localized to the ER and NE when transiently overexpressed (Figure 2A). Mutating residues that preserve the positive charge of the polar face did not affect the NE/ER localization (AH(3R/K)-EGFP; Figure 2A). In contrast, mutating bulky hydrophobic residues (AH(2F/2L/A)-EGFP; Figure 2A) or replacing the positively charged residues (3RK) residues to aspartic acids (AH(3RK/D)-EGFP; Figure 2A) abolished ER and NE membrane targeting. Thus, the positively charged and bulky hydrophobic residues of the N-terminus of CTDNEP1 are necessary for its membrane targeting, which is in line with in silico predictions that this region encodes for a peripheral membrane binding AH.

Selective permeabilization of the plasma membrane by digitonin showed that the C-terminus of CTDNEP1 faces the cytoplasm (Supplemental Figure S2C). In addition, the predicted AH sequence tagged at both the N- and C-terminus localized to the ER and NE in digitonin-permeabilized cells (Supplemental Figure S2, D and E). These data provide further evidence that CTDNEP1 and its N-terminal predicted AH do not cross the membrane.

CTDNEP1-EGFP localized to the rim enclosing a neutral lipid marker in cells treated with excess fatty acids (Figure 2B) and colocalized with some neutral lipid-marked puncta under basal conditions (Supplemental Figure S2F). A CTDNEP1 chimera with its N-terminal AH (aa 3–30) replaced with the *S. Cerevisiae* Nem1 hydrophobic region (aa 87-126; Nem1HR-CTDNEP1) localized to ER and NE (Supplemental Figure S2G), but not to the surface of LDs (Supplemental Figure S2H), consistent with reports in budding yeast showing that Nem1 does not localize to the surface of LDs (Adeyo *et al.*, 2011). We conclude that the N-terminus of CTDNEP1 has evolved to encode a peripheral membrane binding AH critical for its targeting to ER, nuclear envelope and LDs.

ER and nuclear envelope targeting of CTDNEP1 promotes complex formation with NEP1R1 and lipin 1 dephosphorylation

We predicted that membrane targeting of CTDNEP1 is a prerequisite for complex formation with NEP1R1 to promote lipin 1 dephosphorylation. Reciprocal coimmunoprecipitation studies showed weak binding between CTDNEP1-HA without its N-terminal AH (hereafter referred to as ΔAH) and Flag-NEP1R1 (Figure 2C), consistent with the subtle stabilization and only partial ER recruitment of ΔAH in cells also coexpressing NEP1R1 (see Figure 1E). In contrast, the Nem1HR-CTDNEP1 chimeric protein that is constitutively localized to ER/nuclear membrane coimmunoprecipitated with Flag-NEP1R1 (Figure 2D). Stable expression of wild type, but not phosphatase dead (PD), CTDNEP1 and the Nem1HR-CTDNEP1 chimera promoted lipin 1 dephosphorylation and Sun2 stability to a significantly greater extent than ΔAH (Figure 2E). Thus, CTDNEP1 must be membrane-bound to perform its catalytic function to dephosphorylate lipin 1. In line with this, ΔAH showed some activity towards lipin 1 dephosphorylation only in the presence of transiently overexpressed Flag-NEP1R1 (Figure 2F) that partially recruits it to the ER and nuclear envelope (Figure 1E). Thus, both targeting of CTDNEP1 to the ER and NE and complex formation with NEP1R1 are required to promote dephosphorylation of lipin 1 and stabilization of Sun2.

Membrane-bound CTDNEP1 is ubiquitylated and targeted for proteasomal degradation in a p97-dependent manner

The dependence of CTDNEP1 protein levels on the presence of NEP1R1 prompted us to test whether CTDNEP1-NEP1R1 complex formation prevents proteasomal targeting and degradation of CTDNEP1. Treating cells with cycloheximide to prevent protein translation revealed that wild type overexpressed CTDNEP1-HA is short-lived (~50% of the protein was degraded within 1 h; Figure 3, A and B) and that its degradation is slowed by the proteasome inhibitor MG132 (Figure 3, A–C). The degradation of endogenous CTDNEP1 was not as pronounced (~35% of the protein is degraded within 1h; Supplemental Figure S3A), albeit degradation of the minor short-lived pool was dependent on the proteasome (Supplemental Figure S3A). In the absence of its N-terminal ER and NE targeting region, CTDNEP1ΔAH was rapidly degraded by the proteasome (~81% of existing protein remained in 1 h; Figure 3, A–C). These data suggest that preventing membrane targeting of CTDNEP1 to impede its ability to bind NEP1R1 or overexpressing CTDNEP1 to alter the ratio of CTDNEP1 to NEP1R1 renders CTDNEP1 unstable.

Prior large-scale screens identified direct ubiquitylation sites in CTDNEP1 (Rose *et al.*, 2016). Full length (WT) and ΔAH CTDNEP1 coimmunoprecipitated with endogenous ubiquitin under denaturing extraction conditions (Figure 3D). Fusion of full length CTDNEP1 to a deubiquitylating domain that cleaves polyubiquitylated chains increased the protein levels of CTDNEP1 and this was dependent on deubiquitylase catalytic activity (Figure 3E; Schlieker *et al.*, 2007). The fusion protein accumulated in the cytoplasm as well as ER and NE (Supplemental Figure S3B), suggesting that CTDNEP1 protein stability depends on polyubiquitylation. The constitutively membrane-bound Nem1HR-CTDNEP1 chimera (Figure 3F) and CTDNEP1-PD (Supplemental Figure S3C) were degraded at a similar rate as wild type CTDNEP1 when stably overexpressed. Thus,

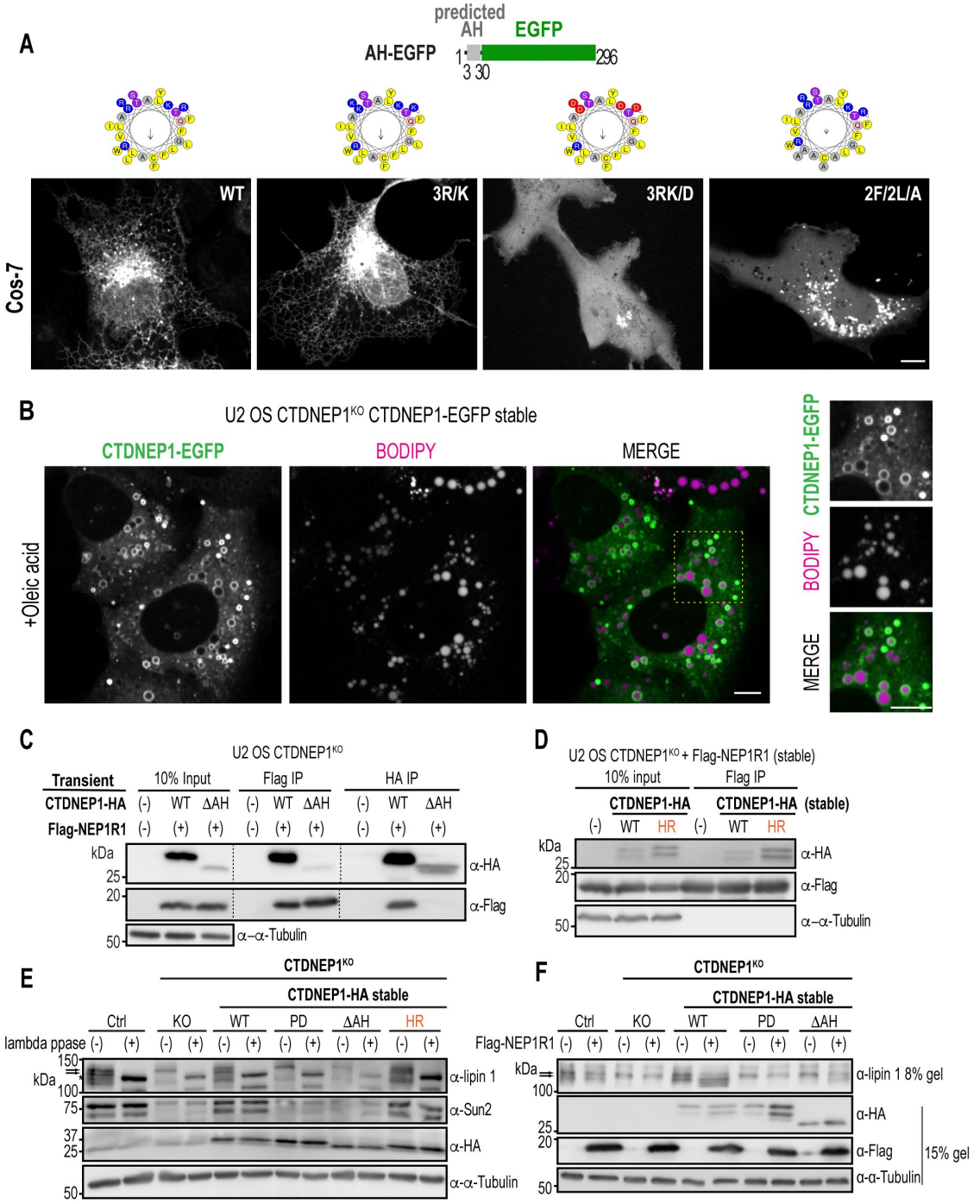

FIGURE 2. Membrane-association of CTDNEP1 promotes binding to NEP1R1 and lipin 1 dephosphorylation. (A) Top: Schematic representations of the N-terminal AH of CTDNEP1 fused to EGFP (AH-EGFP). Bottom: Representative spinning disk confocal images of AH-EGFP mutant variants transiently transfected in living Cos-7 cells. *N* = 2 independent experiments for 3R/K, 3RK/D and 2F/2L/A and 3 for WT. (B) Representative spinning disk confocal images of stably expressed CTDNEP1-EGFP in living U2 OS CTDNEP1 KO cells stained with Bodipy C12 and fed with 200 μM Oleic acid for 24 h. Insets show CTDNEP1-EGFP and the neutral lipid marker, Bodipy C12. *N* = 3 independent experiments. Scale bars, 10μm (C and D) Immunoblot of immunoprecipitations from whole cell lysates of U2 OS CTDNEP1 KO cells transiently coexpressing CTDNEP1-HA variants and Flag-NEP1R1. *N* = 2 independent experiments. (E) Immunoblot of whole cell lysates from CTDNEP1 KO cells stably expressing indicated CTDNEP1-HA variants with or without exogenous lambda phosphatase treatments. *N* = 2 independent experiments. (F) Immunoblot of whole cell lysates from CTDNEP1 KO cells stably expressing CTDNEP1-HA variants and transiently expressing Flag-NEP1R1. *N* = 2 independent experiments. Arrows are lipin 1 phospho-species, asterisks marks lambda phosphatase dephosphorylated lipin 1.

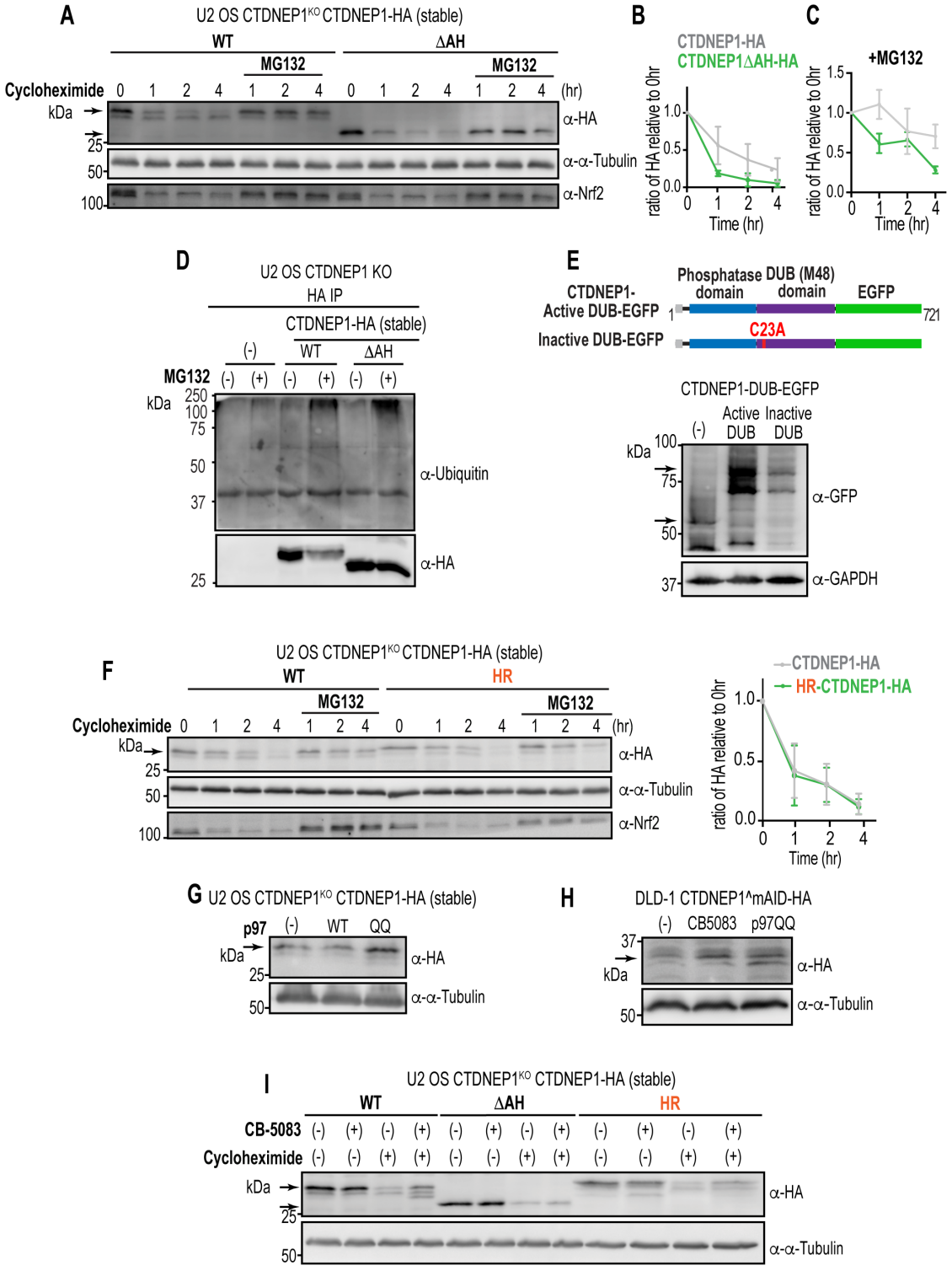

FIGURE 3. Membrane-bound CTDNEP1 is targeted for degradation by the ubiquitin-proteasome system in a p97-dependent manner. (A) Immunoblot of whole cell lysates from CTDNEP1 KO cells stably overexpressing CTDNEP1-HA variants treated with cycloheximide ± MG132 for indicated times. (B and C) Plot represents mean intensity value of top band of CTDNEP1-HA relative to its initial timepoint (0 h) normalized to tubulin in either (B) Cycloheximide or (C) Cycloheximide + MG132 conditions. Mean ± SD shown. *N* = 3 (Cycloheximide + MG132) or 4 (Cycloheximide) independent experiments. (D) Immunoblot of indicated CTDNEP1-HA variants immunoprecipitated with ubiquitin under denaturing conditions from U2 OS CTDNEP1-KO cells treated with MG132 for 4 h to increase ubiquitylated proteins. *N* = 2 independent experiments. (E) Top: Schematic representation of CTDNEP1 fused to the M48 deubiquitylase domain and to EGFP. Bottom: Immunoblot of whole cell lysates from U2 OS cells transiently transfected with the indicated constructs. *N* = 2 independent experiments. (F) Left: Immunoblot of whole cell lysates from CTDNEP1 KO cells stably expressing CTDNEP1-HA variants and treated with cycloheximide ± MG132 for the indicated time course;

membrane-associated CTDNEP1 is a target of proteasomal degradation and this is independent of its catalytic active site.

To visually observe the short-lived subcellular pools of CTDNEP1 protein, we imaged CTDNEP1 knockout cells stably expressing wild type CTDNEP1-EGFP, which is expressed at higher levels than endogenous CTDNEP1^EGFP thus altering the ratio of CTDNEP1 to NEP1R1 (Supplemental Figure S3, D and E). Cycloheximide treatment showed uniform loss of EGFP signal from the ER and NE (Supplemental Figure S3D). In cells additionally treated with MG132, CTDNEP1-EGFP accumulated to punctate structures in the perinuclear region, many of which colocalized with the lysosomal marker Lamp1-mScarlet (Supplemental Figure S3, D and F). Thus, when CTDNEP1 is overexpressed to alter its ratio to NEP1R1 it is mainly downregulated by proteasome-mediated degradation. Trafficking to the lysosome may further prevent its aberrant accumulation at the ER and NE.

We next tested whether the AAA$^+$-ATPase VCP/p97 (Cdc48 in *S. cerevisiae*) protein complex participates in degradation of CTDNEP1. VCP/p97 extracts membrane proteins and cooperates with the proteasome in the ER-associated protein degradation (ERAD) pathway. Overexpression of a dominant negative variant of p97 (p97 QQ) that no longer hydrolyzes ATP (Tsai *et al.*, 2016) increased the protein levels of CTDNEP1-HA stably expressed in CTDNEP1 knockout cells (Figure 3G). p97 inhibition, either by overexpression of the p97 QQ dominant negative construct or by treating cells with a small molecule ATP competitive inhibitor of a domain of p97, also stabilized endogenous CTDNEP1^mAID-HA in DLD-1 cells (Figure 3H). Small molecule inhibition of p97 stabilized existing protein pools of wild type CTDNEP1 and the Nem1HR-CTDNEP1 chimera, but not soluble ΔAH CTDNEP1 (Figure 3I). Thus, a p97-dependent activity is required for the regulated degradation of membrane-bound CTDNEP1.

Interestingly, NEP1R1 is longer-lived, even when overexpressed, than either overexpressed or endogenous CTDNEP1 (Supplemental Figure S4A), suggesting that CTDNEP1, and not the CTDNEP1-NEP1R1 complex, is selectively targeted for proteasomal degradation.

CTDNEP1 and NEP1R1 associate directly through a hydrophobic binding interface

Our data suggested that when CTDNEP1 is not bound to NEP1R1 it is short-lived and degraded in a p97 and proteasomal-dependent manner. To test this, we sought to create mutant versions of either NEP1R1 or CTDNEP1 that disrupt complex formation without disrupting their overall domain architecture and targeting to the ER and NE. AlphaFold three-dimensional modeling of the CTDNEP1/NEP1R1 heterodimer revealed a hydrophobic interface between the proteins consisting of mainly three residues in CTDNEP1 (CTDNEP1 M220, A223, V233) and two residues in NEP1R1 (NEP1R1 F30, L120) with hydrophobic amino acid side chains at its core (Figure 4, A and B). The majority of these interactions, including F30 in NEP1R1 and V233 in CTDNEP1, were recently confirmed by our experimental crystal structure of the CTDNEP1-NEP1R1 complex (Gao *et al.*, 2024). Mutating the bulky, centrally positioned phenylalanine residue (F30) of NEP1R1 to either a small hydrophobic amino acid (F30A) or a charged amino acid (F30E) strongly reduced binding with CTDNEP1-HA, as shown by reciprocal coimmunoprecipitation experiments (Figure 4C). Variants of CTDNEP1-HA in which the hydrophobic V233 was mutated to a charged residue (V233E) or both M220/V233 were mutated to alanine also strongly reduced complex formation with Flag-NEP1R1 (Figure 4D). The ER and NE localization of the mutant versions of either NEP1R1 (Supplemental Figure S4B) or CTDNEP1 (Supplemental Figure S4C) was unaffected compared with the wild type tagged proteins, indicating that a change in subcellular localization does not underlie the lack of complex formation under these conditions.

We next determined whether mutation of the hydrophobic interfaces disrupt direct binding between CTDNEP1 and NEP1R1 in vitro. The AH of CTDNEP1 is required for its membrane targeting to facilitate its stable association with ER-bound NEP1R1; however, CTDNEP1-NEP1R1 complex formation in vitro does not require the AH of CTDNEP1 (Gao *et al.*, 2024). Size exclusion chromatography of in vitro purified CTDNEP1ΔAH (tagged with His-MBP) combined with NEP1R1 coeluted in peak fractions that were shifted relative to CTDNEP1ΔAH or NEP1R1 alone (Figure 4E), indicating that these proteins form a complex. CTDNEP1ΔAH phosphatase activity towards the generic substrate p-NPP confirmed coelution of CTDNEP1 with wild type NEP1R1 (dotted lines in Figure 4E). The peak representing complex formation was absent when the NEP1R1(F30E) mutant was combined with CTDNEP1ΔAH (Figure 4F). Combining active CTDNEP1ΔAH(V233E) with wild type NEP1R1 also did not result in the shifted peak that represents complex formation (Figure 4G), further verifying that the predicted hydrophobic interface formed by these residues facilitates complex formation. Quantitative comparison of the phosphatase activity of CTDNEP1ΔAH(V233E) towards a generic substrate demonstrated that this mutation does not disrupt the catalytic site of CTDNEP1 in vitro (Figure 4H). Thus, our in vitro and in vivo data identified key residues that facilitate CTDNEP1/NEP1R1 complex formation.

NEP1R1 limits the rate of proteasomal degradation of CTDNEP1

The CTDNEP1 and NEP1R1 mutant variants that localize to the ER and nuclear envelope, but are unable to heterodimerize, allowed us to directly test how complex formation influences the stability and functions of CTDNEP1. We first transiently overexpressed wild type Flag-NEP1R1 and found that the majority of existing CTDNEP1-HA protein was stable after 1 h (Figure 5, A and B; ~70% of the protein remains within 1 h). In cells overexpressing NEP1R1(F30E), less than half of existing CTDNEP1-HA remained (Figure 5, A and B), which is similar to the rate of degradation of CTDNEP1-HA in cells that were not transiently overexpressing NEP1R1 (see Figure 3A). Transient overexpression of the NEP1R1(F30E) mutant also did not increase endogenous CTDNEP1^EGFP protein levels (Supplemental Figure S4D). Overexpressed Flag-NEP1R1 was long-lived independent of heterodimer formation (Figure 5A).

Right: Plot represents mean intensity value of top band of CTDNEP1-HA relative to its initial timepoint (0 h) normalized to tubulin. Mean ± SD shown. *N* = 3 independent experiments. (G) Immunoblot of whole cell lysates from CTDNEP1 KO cells stably expressing CTDNEP1-HA and transiently expressing indicated p97 variants. *N* = 2 independent experiments. (H) Immunoblot of whole cell lysates from DLD-1 cells with CTDNEP1 endogenously tagged with mAID-HA, treated with CB-5083 to inhibit p97 or transfected with p97 QQ. *N* = 2 independent experiments. (I) Immunoblot of whole cell lysates from CTDNEP1 KO cells stably expressing indicated CTDNEP1-HA variants and treated with cycloheximide with and without CB-5083 to inhibit p97 for 4 h. *N* = 3 independent experiments.

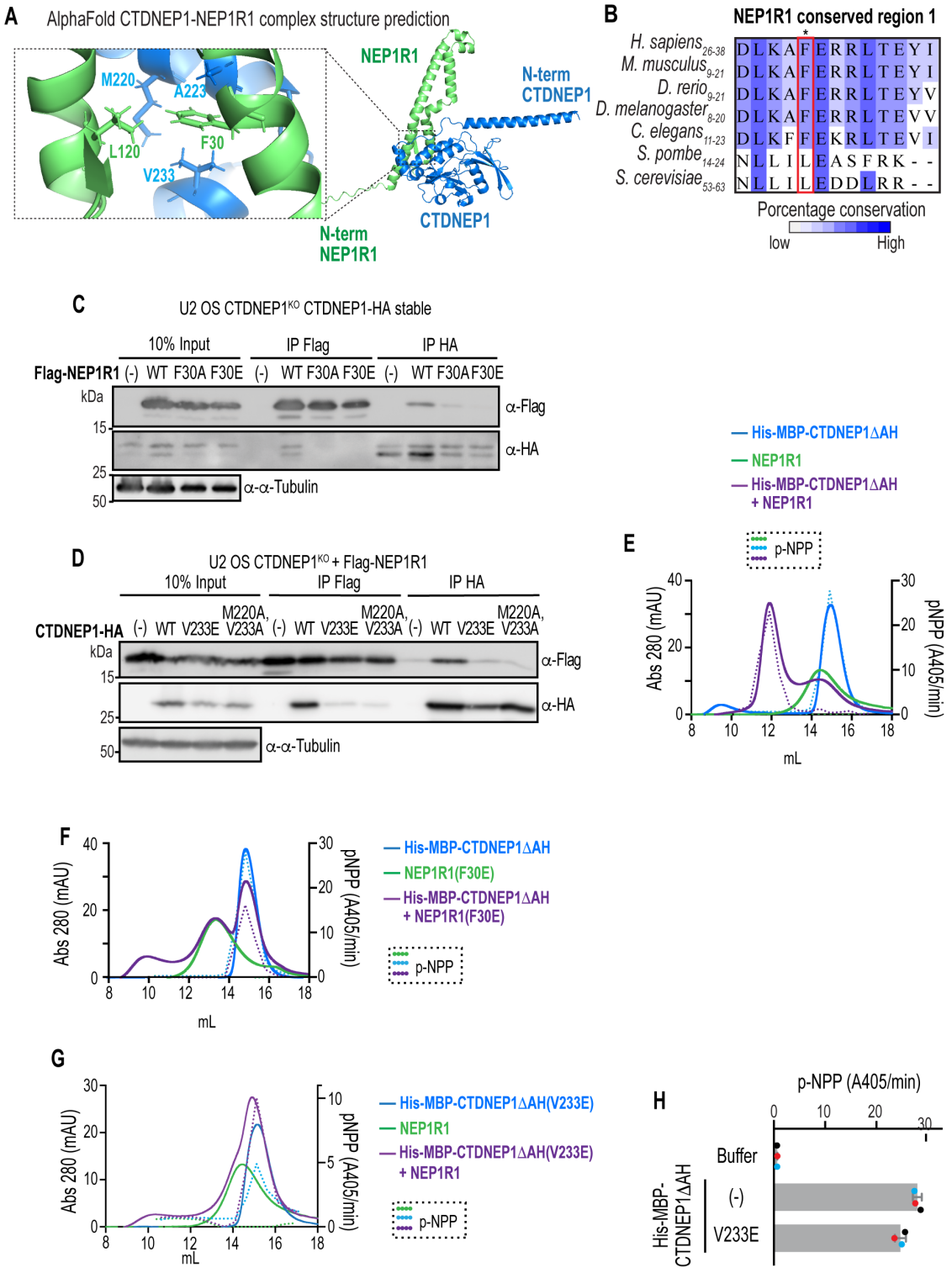

FIGURE 4. The interaction between CTDNEP1 and NEP1R1 in vitro and in vivo depends on a hydrophobic interface. (A) AlphaFold structure prediction of the CTDNEP1-NEP1R1 complex. Zoom-in highlights residues at a binding interface between the proteins. (B) Multiple sequence alignment of NEP1R1 amino acid residues at binding interface with CTDNEP1 based on (A). The metazoan-specific conserved phenylalanine residue is highlighted in a red box. (C) Immunoblot of immunoprecipitated Flag-NEP1R1 variants with CTDNEP1-HA in U2 OS CTDNEP1-deleted cells stably expressing CTDNEP1-HA and transfected with mutant variants. $N = 2$ independent experiments. (D) Immunoblot of immunoprecipitated CTDNEP1-HA mutant variants with Flag-NEP1R1 in U2 OS CTDNEP1 deleted cells transiently expressing indicated proteins. $N = 2$ independent experiments. (E–G) Size exclusion chromatography of purified His6-MBP-CTDNEP1ΔAH and NEP1R1 variants. Solid lines are the elution profiles of the proteins and dotted lines are the pNPP assay results. (H) pNPP assay of His6-MBP-CTDNEP1ΔAH and NEP1R1 variants normalized for comparison. Mean ± SD shown. $N = 3$ independent experiments.

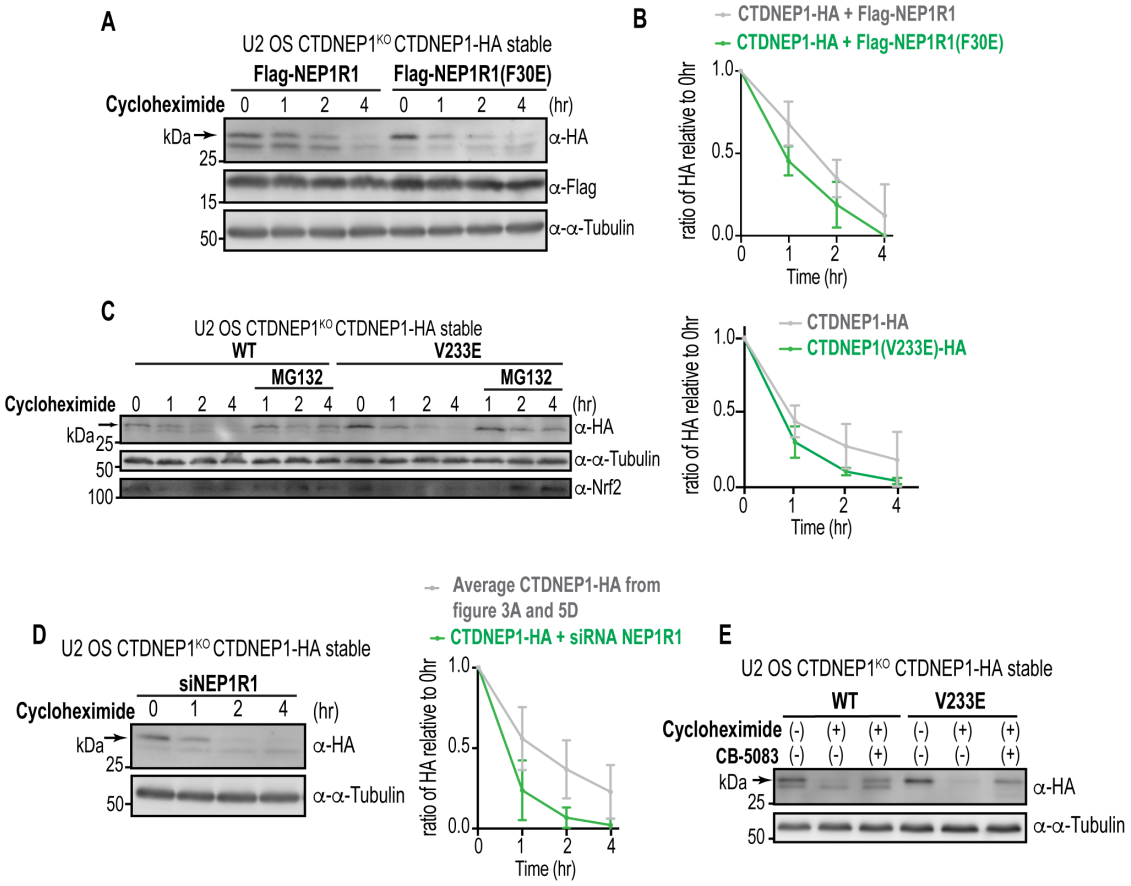

FIGURE 5. NEP1R1 is longer-lived and stabilizes CTDNEP1 from proteasomal degradation. (A) Immunoblot of whole cell lysates of CTDNEP1-deleted cells stably expressing CTDNEP1-HA transfected with Flag-NEP1R1 variants and treated with cycloheximide for the indicated time course. (B) Plot represents mean intensity value of top band of CTDNEP1-HA relative to its initial timepoint (0 h) normalized to tubulin. Mean ± SD shown. *N* = 3 independent experiments. (C) Left: Immunoblot of whole cell lysates of CTDNEP1-deleted cells stably expressing CTDNEP1-HA mutant variants and treated with cycloheximide ± MG132 for the indicated time points. Right: Plot represents mean intensity value of top band of CTDNEP1-HA relative to its initial timepoint (0 h) normalized to tubulin. Mean ± SD shown. *N* = 3 independent experiments. (D) Left: Immunoblot of whole cell lysates of CTDNEP1-deleted cells stably expressing CTDNEP1-HA, RNAi-depleted of endogenous NEP1R1 and treated with cycloheximide for indicated time points. Right: Plot represents mean intensity value of top band of CTDNEP1-HA relative to its initial timepoint (0 h) normalized to tubulin. Mean ± SD shown. *N* = 3 (RNAi NEP1R1) or 7 (CTDNEP1-HA from 3A and 5D) independent experiments. (E) Immunoblot of whole cell lysates of CTDNEP1-deleted cells stably expressing CTDNEP1-HA variants treated with cycloheximide and/or CB-5083 to inhibit p97 for 4 h. *N* = 3 independent experiments.

We next assessed the degradation rate of CTDNEP1 in cells RNAi-depleted for NEP1R1 and of the CTDNEP1(V233E) mutant that is significantly reduced in its binding to NEP1R1. In both cases, CTDNEP1 not bound to NEP1R1 is very short-lived (only ~30% of the protein remains within 1 h; Figure 5, C and D), further confirming the effect of NEP1R1 on stabilizing CTDNEP1 in vivo. Furthermore, p97 activity is required for degradation of existing CTDNEP1(V233E)-HA protein (Figure 5E), suggesting that p97 extracts CTDNEP1 from membranes when it is not bound to NEP1R1. Together, our data suggest that NEP1R1 acts as an ER and NE associated scaffold that shelters membrane-bound CTDNEP1 from proteasomal degradation.

NEP1R1 regulates the stability of CTDNEP1 to restrict ER membrane expansion

CTDNEP1 activity is required to limit ER membrane biogenesis through lipin 1 dephosphorylation (Merta *et al.*, 2021). While our data in cells show that membrane association of CTDNEP1 promoted lipin 1 dephosphorylation, it remained unclear whether this function relies on direct binding of CTDNEP1 with NEP1R1. The CTDNEP1(V233E)-HA mutant that was active in vitro (see Figure 4G) and localized to ER-nuclear membranes, but did not bind to NEP1R1 (see Figure 4, D and H; Supplemental Figure S4C) provides a tool to test whether direct CTDNEP1-NEP1R1 association in cells is required for lipin 1 dephosphorylation. In CTDNEP1 knockout cells stably expressing CTDNEP1(V233E), lipin 1 was not dephosphorylated to the same extent as cells expressing wild type CTDNEP1 or the Nem1HR CTDNEP1 chimera (Figure 6A). In line with the reduction in lipin 1 dephosphorylation, Sun2 levels were not stabilized with the CTDNEP1(V233E) mutant (Figure 6A). Furthermore, the CTDNEP1ΔAH and V233E mutants did not support nuclear translocation of lipin1β-GFP upon inhibition of mTORC1 (Supplemental Figure S5, A and B). Expression from a constitutive promoter increased the steady-state protein levels of the V233E mutant, but this was not sufficient for lipin 1 dephosphorylation and Sun2 stability (Figure 6A), because of the lack of NEP1R1 complex formation. We conclude that in addition to

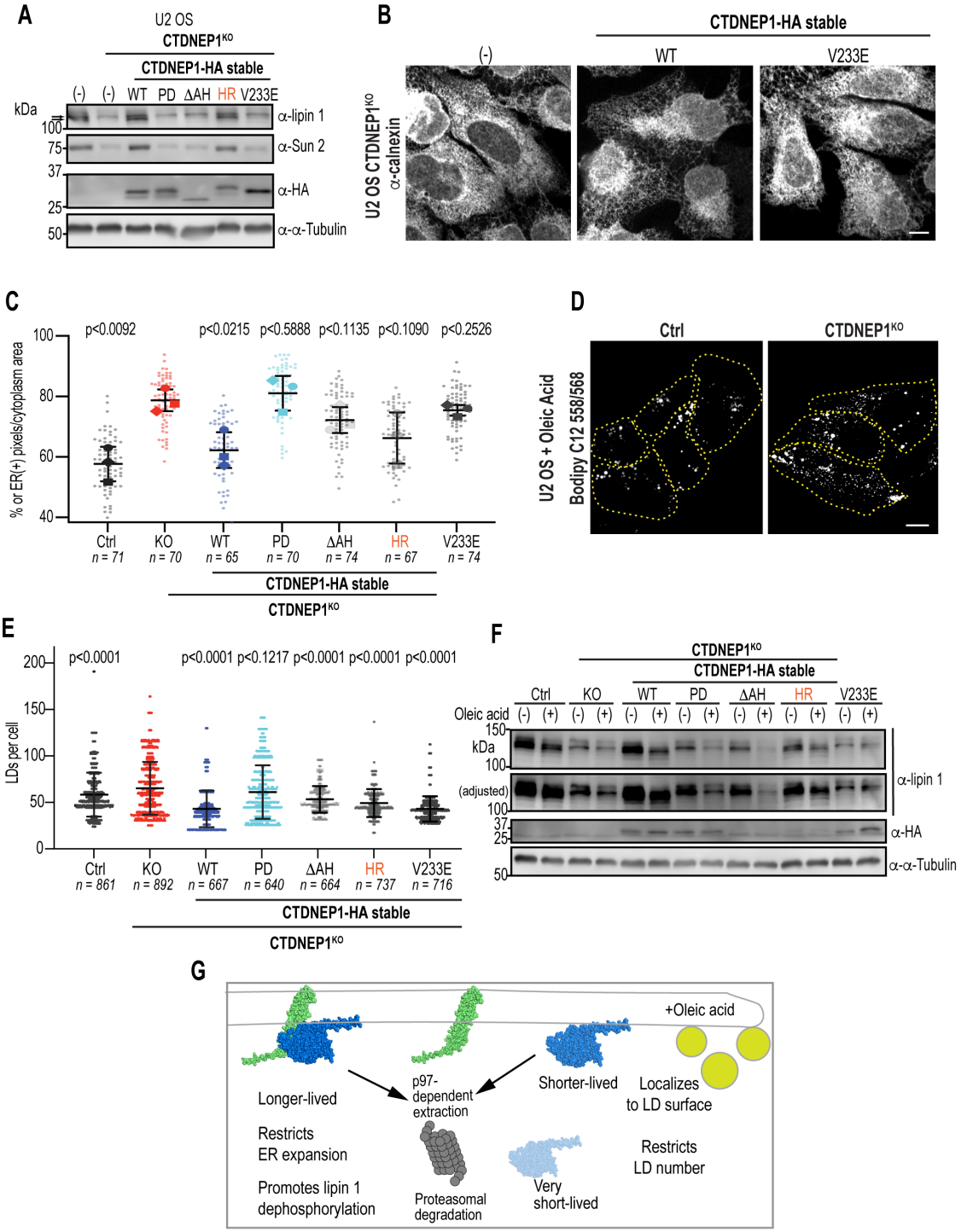

FIGURE 6. CTDNEP1 complex formation with NEP1R1 restricts ER membrane expansion but is not required for CTDNEP1's role in limiting lipid droplet biogenesis. (A) Immunoblot of whole cell lysates of CTDNEP1 deleted cells stably expressing CTDNEP1-HA mutant variants. $N = 3$ independent experiments. (B) Representative spinning disk confocal images of calnexin immunostaining in fixed U2 OS CTDNEP1-deleted cells stably expressing CTDNEP1-HA variants. (C) Plot represents percent area of calnexin fluorescence signal (cell area subtracted by nuclear area) for cells from indicated cells. Individual data points and mean ± SD shown. $N = 3$ independent experiments; p values are paired t tests of replicate mean; all p values are relative to U2 OS CTDNEP1-deleted cells. (D) Representative spinning disk confocal images of Bodipy C12 staining in living U2 OS and U2 OS CTDNEP1-deleted cells treated with oleic acid for 24 h. Dotted lines indicate the edges of the cells. (E) Plot represents quantification of the number of LDs per cell in the indicated cells using semiautomated algorithm. Mean ± SD shown. $N = 4$ (Ctrl and CTDNEP1 deleted cells) or 5 (CTDNEP1-HA stable variants) independent experiments. P values, One-way Anova with Dunnet's multiple comparisons test, all p values are relative to CTDNEP1-deleted cells. (F) Immunoblot of whole cell lysates of CTDNEP1-deleted cells stably expressing CTDNEP1-HA mutant variants treated with Oleic acid for 24 h. $N = 2$ independent experiments. (G) Schematic representing different pools of CTDNEP1 and their relative stabilities and roles in lipid synthesis. For all: Scale bars, 10 μm. n = individual cells counted.

protection from proteasomal degradation, NEP1R1 binding promotes CTDNEP1 activity and functions in vivo.

The extent at which different mutant variants of CTDNEP1 promoted lipin 1 dephosphorylation correlated with the ability to rescue the increase in ER size and defects in nuclear solidity resulting from loss of CTDNEP1 (Figure 6, B and C; Supplemental Figure S5, C–E). Thus, complex formation with NEP1R1 is necessary for CTDNEP1 to restrict ER membrane biogenesis through lipin 1 regulation. In line with this, siRNA depletion of endogenous NEP1R1 results in ER expansion (Supplemental Figure S5, F–H; Gao *et al.*, 2024), and this is rescued by expression of siRNA resistant wild type, but not F30E Flag-NEP1R1 (Figure S5, F–H). We conclude that binding to NEP1R1 is essential for CTDNEP1 to perform its function in regulating ER membrane biogenesis in cells.

CTDNEP1 controls lipid droplet number independent of NEP1R1 binding

Previous work showed that oleate treatment promotes dephosphorylation of lipin 1 and translocation to membranes (Harris *et al.*, 2007; Kim *et al.*, 2007). In BHK cells, overexpression of CTDNEP1 led to dephosphorylation of lipin 1 in the presence of oleate (Kim *et al.*, 2007). This result suggested that NEP1R1 coexpression may not be required for oleate-induced lipin 1 dephosphoryaltion by CTDNEP1. However, in budding yeast, overexpression of human CTDNEP1 with NEP1R1, but not overexpression of human CTDNEP1 alone, restored reduced TAG synthesis in *spo7*Δ or *nem1*Δ*spo7*Δ mutants (Han *et al.*, 2012). Thus, there may be differences from yeast to humans in the reliance of CTDNEP1 on NEP1R1 in the presence of oleate.

We set out to test whether CTDNEP1-NEP1R1 complex formation has a role in LD biogenesis in cells fed with oleate using our mutant constructs. CTDNEP1 knockout cells contained a greater number of LDs per cell, and this was dependent on its phosphatase active site (Figure 6, D and E). Overexpression of WT CTDNEP1 and all of the mutant variants (Nem1HR, ΔAH, and V233E), except for PD, restored the increase in lipid droplet number resulting from loss of CTDNEP1 (Figure 6E). Interestingly, the CTDNEP1(V233E) mutant that is significantly reduced in NEP1R1 binding rescued lipid droplet number to the same extent as wild type CTDNEP1 levels ($p < 0.9999$ relative to WT CTDNEP1; Figure 6E), whereas the Nem1HR and ΔAH variants restored lipid droplet number to a lesser extent ($p < 0.0001$ relative to WT CTDNEP1 for both; Figure 6E). We observed the appearance of faint faster migrating endogenous lipin 1 species induced by oleic acid treatment in all conditions except for CTDNEP1 knockout cells and CTDNEP1-PD expressing cells (Figure 6F). This suggested that NEP1R1 binding and membrane association are not required for oleic-acid stimulated dephosphorylation of lipin 1. The protein levels of lipin 1 are lower in the ΔAH and V233E mutant conditions (Figure 6F) suggesting that the effect of CTDNEP1 on lipin 1 stability may be through a distinct mechanism that still requires membrane and NEP1R1 binding. Together, these results indicate that CTDNEP1 limits the number of LDs per cell under conditions of excess oleic acid, however this function is independent of NEP1R1 binding and partially dependent on its AH when overexpressed.

In sum, ER and nuclear envelope targeting as well as NEP1R1 binding of CTDNEP1 are required to limit ER membrane synthesis, promote lipin 1 dephosphorylation, maintain nuclear shape and stabilize Sun2 protein levels. CTDNEP1 also restricts lipid droplet formation; however, this function does not strictly require NEP1R1 binding. We conclude that under conditions of excess fatty acids, CTDNEP1 function may be rewired to restrict lipid droplet biogenesis providing evidence for context-dependent regulation and function of CTDNEP1.

DISCUSSION

We demonstrate that different mechanisms are involved in the targeting and stabilization of CTDNEP1. These mechanisms coordinately regulate membrane-bound CTDNEP1 to promote lipin 1 dephosphorylation for limiting ER membrane expansion. An N-terminal AH in CTDNEP1 targets it to the ER and nuclear envelope where CTDNEP1 is either degraded by the proteasome or stabilized through its interaction with NEP1R1 (Figure 6G). We mutated a key interaction interface in CTDNEP1 and NEP1R1 to show the importance of NEP1R1 binding in promoting the phosphatase activity of CTDNEP1 towards lipin 1. We show that the CTDNEP1-NEP1R1 complex is responsible for counteracting mTORC1-mediated cytoplasmic retention of lipin 1. Interestingly, CTDNEP1 localized to LDs and its activity limited oleic-acid induced lipid droplet biogenesis; however, its mode of regulation for LD biogenesis no longer involved NEP1R1 binding. Thus, regulation of the CTDNEP1-NEP1R1 complex may be rewired in the presence of excess exogenous fatty acids so that CTDNEP1 can support LD biogenesis independent of NEP1R1.

We show that the majority of endogenous CTDNEP1 is stabilized by NEP1R1 under basal conditions. Altering the ratio of CTDNEP1 to NEP1R1 by overexpressing CTDNEP1 alone resulted in the rapid proteasomal degradation of CTDNEP1. NEP1R1 is relatively more stable than CTDNEP1, even when overexpressed, and is constitutively localized to the ER and nuclear envelope. We suggest that NEP1R1 acts as an membrane scaffold for CTDNEP1 stabilization. This is in line with our recent work showing that NEP1R1 allosterically stabilizes and activates overexpressed CTDNEP1 by binding to a hydrophobic surface that is unique among human CTD phosphatases and distant from the active site (Gao *et al.*, 2024). The fact that overexpressed CTDNEP1 does not require NEP1R1 for its LD localization or function in oleate-induced LD biogenesis suggests that the hydrophobic surface of CTDNEP1 normally occupied by NEP1R1 may be stabilized through a different mechanism at LDs. In yeast, several posttranslational events as well as protein binding partners have been shown to disrupt formation of the Nem1/Spo7 complex during the cell cycle (Su *et al.*, 2018; Dey *et al.*, 2019; Papagiannidis *et al.*, 2021; Saik *et al.*, 2023). In the case of mammalian cells, the switch from membrane biogenesis to lipid storage may promote disruption of the CTDNEP1-NEP1R1 complex (or prevent its formation) to allow LD localization and associated functions of CTDNEP1.

Increasing evidence shows that crosstalk between the ER-associated ubiquitin proteasome pathway and regulation of lipid synthesis maintains ER lipid homeostasis (Stevenson *et al.*, 2016; Olzmann and Carvalho, 2019). We show that when not associated to NEP1R1, ER-bound CTDNEP1 is degraded through mechanisms that resemble the ERAD pathway (Christianson *et al.*, 2023). LDs are associated with p97 activity but lack the canonical ERAD machinery (Stevenson *et al.*, 2016), so it will be interesting to determine the stability of the LD-associated pool of CTDNEP1 at this subcellular location.

The role of CTDNEP1 in counteracting mTOR-mediated lipogenesis and the emergence of CTDNEP1 as a tumor suppressor underscores the importance of understanding how CTDNEP1 performs its functions in regulated lipid synthesis (Jones *et al.*, 2012; Luo *et al.*, 2023). CTDNEP1 and its metazoan homologues participate in many nuclear envelope-dependent processes through lipin regulation (Han *et al.*, 2012; Bahmanyar *et al.*, 2014; Penfield *et al.*, 2020; Lee *et al.*, 2023). CTDNEP1 is also implicated in BMP signaling and in regulation of neural tube development suggesting

potential context-dependent differences in its function (Satow *et al.*, 2006; Sakaguchi *et al.*, 2013; Darrigrand *et al,*. 2020). Moreover, metabolic disorders associated with lipin deficiency motivate further understanding of its regulation by CTDNEP1 (Reue, 2009). In sum, understanding how CTDNEP1 executes its functions and how CTDNEP1-NEP1R1 complex formation is regulated is broadly important to our understanding of cellular functions and disease.

MATERIALS AND METHODS

Request a protocol through *Bio-protocol*.

Mammalian cell lines

U2 OS, Cos 7, DLD-1 and HEK293-T cells were obtained the source specified. Cells were grown at 37°C in 5% CO_2 in DMEM low glucose (Life Technologies 11885) supplemented with 10% heat inactivated fetal bovine serum (FBS; F4135) and 1% antibiotic-antimycotic (Life Technologies 15240112). Cells were cultured without antibiotics during transfections, RNAi, and treatments for experiments. Cells were used for experiments before passage 25. Cells were tested for mycoplasma upon initial thaw and generation of new cell lines (Southern Biotech 13100-01), and untreated cells were continuously profiled for contamination by assessment of extranuclear DAPI/Hoechst 33258 staining.

Stable cell line generation

U2OS CTDNEP1^{KO} + CTDNEP1 stable cell lines (CTDNEP1(V233E)-HA, Nem1HR-CTDNEP1-HA, CTDNEP1ΔAH-HA, CTDNEP1-EGFP, CTDNEP1(V233E)-EGFP) were generated by retroviral transduction, and bulk populations of cells were used for experiments. Retroviruses were generated by transfecting HEK293T cells with pCG-gag-pol, pCG-VSVG and pMRX-CTDNEP1 using Lipofectamine 2000. The retroviruses were recovered 48 h posttransfection, filtered using a 0.22 um PVDF syringe filter and used to transduce U2OS CTDNEP1^{KO} cells. After 48 h of infection, cells were placed under 7.5 µg/ml blasticidin selection for ~1 wk or until control cells where dead, then frozen and/or used for experiments. Cells were continuously cultured in 7.5 µg/ml blasticidin.

Transfection and RNAi

Transfections of cells for fix or live imaging were performed with Lipofectamine 2000 (Thermo Fisher Scientific 11668) in Opti-MEM (Life Technologies 31985) using a 1:2 ratio of DNA:lipofectamine with DNA concentrations ranging from 0.05–0.3 µg DNA per cm^2 of growth surface. Briefly, DNA and lipofectamine were added to 10 µl OptiMEM per cm^2 of growth surface in separate borosilicate glass tubes (Thermo Fisher Scientific STT-13100-S). After 5-min incubation, DNA solution was added to lipofectamine solution. After 15 min, DNA:lipofectamine mix was added dropwise to cells plated 16–24 h before transfection in fresh antibiotic-free media (1 ml/9.6 cm^2 growth surface). Media was exchanged for antibiotic-free media after 6 h.

Transfections of cells for immunoblotting were performed with Polyjet (SL100688) in high glucose DMEM (11965092) using a 1:3 ratio of DNA:Polyjet with DNA concentrations ranging from 0.1 µg DNA per cm^2 of growth surface. Briefly, DNA and Polyjet were added to 10 µl high glucose DMEM per cm^2 of growth surface in separate borosilicate glass tubes (Thermo Fisher Scientific STT-13100-S). After 5-min incubation, Polyjet solution was added to DNA solution. After 10 min, DNA:Polyjet mix was added dropwise to cells plated 16–24 h before transfection in fresh antibiotic-free media (1 ml/9.6 cm^2 growth surface). Media was exchanged for antibiotic-free media after 6 h.

For experiments involving transient CTDNEP1 and/or NEP1R1 overexpression, pcDNA3.0 was used as an empty vector negative control.

RNAi was performed using Dharmafect 1 (Horizon Discovery T-2001) in Opti-MEM according to the manufacturer's protocol for 20 nM. RNAi performed for immunoblot or imaging was analyzed after 48–72 h.

Plasmid generation

General note. Insertion of gene sequence was conducted either by using restriction enzymes from New England Biolabs, Gibson Assembly (New England Biolabs E5510S) or In-Fusion HD Cloning Plus (Takara 638909). Site-directed mutagenesis was performed by QuickChange Site-directed Mutagenesis Kit (Agilent 200523). Multi-site-directed mutagenesis was performed by QuikChange Multi site-directed Mutagenesis Kit (Agilent 200513). Successful cloning was confirmed by sequencing for all constructs.

Point mutagenesis

CTDNEP1 point mutagenesis was modified from pcDNA or pMRX CTDNEP1-HA or CTDNEP1-GFP using Quickchange Mutagenesis to make the following mutations: V233E, M220A/V233A. NEP1R1 point mutagenesis was modified from pRK5-Flag-NEP1R1 using Quickchange Mutagenesis to make the following mutations: F30E, F30A. For CTDNEP1 region deletions, PCR was performed removing the region of interest followed by In-Fusion (Takara 638909).

Region deletions and chimeras

For deletion of CTDNEP1's N-terminus, PCR was performed using primers to amplify the plasmid without the N-terminus, followed by In-Fusion. For Nem1HR-CTDNEP1, PCR was performed with primers deleting the AH and overhangs coding for *yeast* Nem1 hydrophobic region, followed by T4 ligation (M0202).

Stable cell cloning

pMRX-EGFP-Blast was enzyme digested with BamHI and NotI-HF and gel purified to remove EGFP. pcDNA-CTDNEP1-EGFP were PCR amplified and T4 ligated into the opened backbone of pMRX-Blast to make pMRX-CTDNEP1-EGFP-Blast. pMRX-CTDNEP1-Blast was subsequently cloned for making point mutations or region deletions has described previously.

Treatments

Drug/compound treatment was done as follows: Cycloheximide 100 µg/ml; MG132 30 µM; CB-5083 5 µM; Oleic acid 200 µM; Torin 1 250 nM; Bafilomycin A1 100 µM. Vehicle control was prepared by diluting the same amount of DMSO as the drug treatment counterpart.

Cycloheximide treatment assay

Cell media was exchanged with 100 µg/ml cycloheximide. After the indicated time, cells were collected for western blot. Using Image lab, band intensity was measured using the volume tool. Mean intensity was subtracted from background and immunoblot intensity of HA-tag was quantified and normalized to that of α-tubulin, and is shown as percentage of the value relative to 0 h.

Quantitative real-time PCR

RNA was harvested using the RNeasy Mini kit (Qiagen 74104) using the manufacturer's protocol, using Qiashredder columns (Qiagen 79654) for tissue homogenization and with additional RNase-free DNase (Qiagen 79254) treatment after the first RW1 wash and

subsequently adding another RW1 wash. RNA was eluted with RNAse-free water and diluted to 50 ng/µl. RNA was subject to reverse transcription using the iScript Reverse Transcription Supermix (Bio-Rad 1708840) with 400 ng RNA per reaction. The subsequent cDNA was diluted 1:5 for RT-qPCR. cDNA was analyzed for RT-qPCR using the iTaq universal SYBR Green Supermix (Bio-Rad 1725120). Cycle threshold values were analyzed using the Δ ΔCt method. Statistical testing was performed on ΔCt values.

Immunofluorescence

Cells were washed 2x with warm phosphate-buffered saline (PBS) and fixed in 4% paraformaldehyde (+0.1% glutaraldehyde for ER structure analyses) in PBS for 15 min, permeabilized in 0.5% Triton X-100 for 5 min (or 30 mg/ml Digitonin for 10 min in ice), then washed three times with PBS and blocked in 2% bovine serum albumin (BSA) in PBS for 30 min. Samples were transferred to a humidity chamber and incubated with primary antibodies in 2% BSA in PBS for 1 h at room temperature with rocking. Samples were washed with PBS three times for 5 min, then incubated with secondary antibodies in 2% BSA in PBS for 1 h at room temperature in the dark with rocking. Samples were then washed with PBS three times for 5 min in the dark. Coverslips were mounted with ProLong Gold Antifade reagent + DAPI (Thermo Fisher P36935) and sealed with clear nail polish.

Immunoblot

Lysis buffers used: 0.1% Triton X-100, 50 mM NaF, 1 mM EDTA, 1 mM EGTA, 10 mM Na2HPO4,50 mM b-glycerophosphate, 1 tablet/50 ml cOmplete protease inhibitor cocktail, pH 7.4, RIPA buffer (25 mM Tris pH 7.4, 1% NP-40, 0.5% sodium deoxycholate, 0.1% SDS, 150 mM NaCl, and 1 tablet/50 ml cOmplete Mini protease inhibitor cocktail [Roche 11836153001]). Cell lysates were removed from growth surfaces by scraping with a rubber policeman after incubation in lysis buffer or by adding lysis buffer to cell pellets collected by trypsinization and centrifugation at 300 × *g* for 5 min followed by one to two PBS washes. Lysates were homogenized by pushing through a 23G needle 30 times and then centrifuged at >20,000 × *g* for 10 min at 4C, then protein concentration was determined using the Pierce BCA Protein assay kit (Thermo Scientific 23225). Twenty to thirty milligrams of whole cell lysates/lane were run on 8–15% polyacrylamide gels dependent on target size, and protein was wet transferred to 0.22-mm nitrocellulose. Ponceau S staining was used to visualize transfer efficiency, then washed with Tris-buffered saline (TBS) or DI water; then, membranes were blocked in 5% nonfat dry milk or BSA in TBS for 1 h. Membranes were then incubated with primary antibodies in 5% milk or BSA for 1–2 h at room temperature or overnight at 4C with rocking. Membranes were washed three times for 5 min in TBS-T, then incubated with anti-HRP secondary antibodies in 5% milk or BSA in TBS-T for 1 h at room temperature with rocking. Membranes were washed three times for 5 min in TBS-T. Clarity or Clarity Max ECL reagent (Bio-Rad 1705060S, 1705062S) was used to visualize chemiluminescence, and images were taken with a Bio-Rad ChemiDoc or ChemiDoc XRS+ system. Exposure times of images used for analysis or presentation were maximum exposure before saturation of pixels around or within target bands.

Antibody concentrations used: Mouse anti-a tubulin DM1A 1:5000; Mouse anti-Flag 1:4000; Rabbit anti-HA 1:1000; Rabbit antilipin 1 1:2000; mouse antimyc 1:1000; rabbit anti-Sun2 1:1000; mouse anti-GFP 1:1000; mouse anti-GAPDH 1:1000; rabbit anti-LC3B 1:1000; rabbit anti-NRF2 1:1000, anti-Ubiquitin HRP 1:1000. all secondaries 1:10000.

Immunoprecipitation

Cell where pelleted by trypsinization and centrifugation at 300x *g* for 5 min followed by 1x PBS wash, after pelleting the cells, they were lysed by adding lysis buffer (0.1% Triton X-100, 50 mM NaF, 1 mM EDTA, 1 mM EGTA, 10 mM Na_2HPO_4, 50 mM β-glycerophosphate, 1 tablet/50 ml cOmplete protease inhibitor cocktail [Roche 11836153001], pH 7.4). Lysates were homogenized by pushing through a 23G needle 30 times and then centrifuged at >20,000 × *g* for 10 min at 4°C. Preconjugated anti-HA magnetic beads (Thermo Scientific 88836) or preconjugated anti-Flag magnetic beads (Sigma M8823) were washed twice with TBST and equilibrated in lysis buffer without detergent. Ten percent of the total volume of lysed cells was transferred to a new tube labeled input, the remaining 90% volume was added to equilibrated beads and incubated for 2 h rocking at 4°C. Anti-HA beads were then washed twice with TBST and 4x loading dye was added to denature the beads and load samples to SDS–PAGE gel. Anti-Flag beads were washed twice with TBS-T, incubated for 30 min with a Flag peptide (ApexBio A6001) and later boiled/loaded into SDS–PAGE gel.

Ubiquitin assay

Cells at around 80% confluency in a 10-cm dish were lysed in RadioImmunoPrecipitation Assay (RIPA) lysis buffer (50 mM Tris–HCl pH 7.5, 150 mM NaCl, 1% Triton X- 100, 0.5% sodium deoxycholate, 0.1% sodium dodecyl sulfate [SDS]) containing NEM (5 mM) and cOmplete protease inhibitor cocktail (Roche). Cell suspension was solubilized on a rotating wheel for 2 h at 4°C. Cell debris were pelleted at 20,000 × *g* for 15 min at 4°C. Supernatants were incubated for 2 h with preequilibrated 30 µl anti-HA antibody magnetic beads. After three 15-min washes in RIPA buffer on a rotating wheel at 4°C, proteins were eluted from the beads in 1 × sample buffer for 15 min at 65°C and collected into fresh tubes using magnetic racks. Eluates were subsequently supplemented with 100 mM DTT (Krshnan *et al.*, 2022).

pNPP assay

One hundred millimeter pNPP was prepared in 50 mM HEPES, pH6.7, 100 mM NaCl, 10 mM MgCl2, 10 mM beta-mercaptoethanol. The reactions were carried out in 96-well plate by mixing 95 µl pNPP solution with 5 µl enzyme (0.1 µM final concentration), and the absorbance at 405 nm were monitored with SpectraMax M2e Microplate Readers (Molecular Devices) at 30-s interval at ambient temperature for 30 min.

In vitro interaction of His6-MBP-CTDNEP1DAH with NEP1R1

Purified His6-MBP-CTDNEP1DAH or His6-MBP-CTDNEP1 DAH(V233E; 12 µm final concentration) were mixed with NEP1R1 or NEP1R1(F30E; 53 µm final concentration), incubated on ice for 3 h, and centrifuged at 15000 rpm for 15 min at 4C. The supernatant was loaded onto Superdex200 increase (10/300). Phosphatase activity of each fraction was analyzed by pNPP assay.

Live cell imaging

For live imaging, cells were plated in ibidi 2 well imaging chambers (ibidi 80287) or ibidi 8 well imaging chambers (ibidi 80827) with DIC lid (ibidi 80055). Samples were imaged in a CO_2-, temperature-, and humidity-controlled Tokai Hit Stage Top Incubator. Objectives were also heated to 37°C. For CO_2-controlled imaging, the imaging media used was Fluorobrite DMEM (Life Technologies A1896701) supplemented with 10% FBS.

Microscopy

Samples for fix imaging of ER, digitonin vs triton permeabilization and samples for live-cell microscopy of localization of CTDNEP1 with other markers were imaged on an inverted Nikon Ti microscope equipped with a Yokogawa CSU-X1 confocal scanner unit with solid state 100-mW 488-nm and 50-mW 561-nm lasers, using a 60 × 1.4 NA plan Apo objective lens (or 10 × 0.25 NA ADL objective with 1.5x magnification), and a Hamamatsu ORCA R-2 Digital CCD Camera.

Samples for live cell imaging of CTDNEP1-EGFP stable siRNA or CTDNEP1 for cells treated with oleate for function in lipid droplet analysis were imaged on an inverted Nikon Ti Eclipse microscope equipped with a Yokogawa CSU-W1 confocal scanner unit with solid state 100 mW 405, 488, 514, 594, 561, 594, and 640-nm lasers, using a 60 × 1.4 NA plan Apo objective lens and/or 20x plan Fluor 0.75 NA multi-immersion objective lens, and a prime BSI sCMOS camera.

Oleate treatment and lipid droplet staining

Oleic acid (oleate) was conjugated to fatty acid free BSA at a molar ratio of 6:1. For experiments of CTDNEP1 localizing to LDs, 200 μM oleate and 0.5 μM BODIPY 558/568 C12 was added in Fluorobrite DMEM (Life Technologies A1896701) supplemented with 10% FBS and imaged after 24 h. For functional experiments of LDs number and area, cells were treated with 200 μM oleate and 1 μM BODIPY 558/568 C12 for 24 h, next day media was changed to Fluorobrite DMEM supplemented with 10% FBS and imaged immediately.

Protein modeling

Protein complex structure prediction was performed using ChimeraX plug-in into google collab for complex structure prediction. Protein prediction outputs where modelled/analyzed using PyMOL education software.

AH predictions

HeliQuest was used to generate a helical wheel projection and to obtain hydrophobic moment <μH> and net charge Z values, which yielded a discriminant factor D = 0.944 (<μH>) + 0.33 (z) as described in HeliQuest (https://heliquest.ipmc.cnrs.fr/HelpProcedure.htm).

Conservation score analysis

For CTDNEP1 AH alignment amino acid sequences were obtained from uniprot and species were chosen such that they include *Saccharomyces cerevisiae (P38757), Caenorhabditis elegans (Q20432), Drosophila melanogaster (Q9VRG7), Homo sapiens (O95476), Mus musculus (Q3TP92), Danio rerio (Q5U3T3)*. For NEP1R1 sequence alignment species were chosen to include *S. cerevisiae (P18410), Schizosaccharomyces pombe (Q9USQ0), C. elegans (Q9XXN3), D. melanogaster (Q8T0B1), H. sapiens (Q8N9A8), M. musculus (Q3UJ81), D. rerio (Q561 × 0)*. A multiple sequence alignment and phylogenetic tree were generated using Clustal Omega with the default settings.

Image analysis

Image analysis was performed using FIJI/ImageJ. For all scoring phenotypes quantified by categorization were scored blindly. Images were blinded for analysis using the ImageJ

Macro ImageJ Filename_Randomizer, cells where randomized and analysis was done blindly. For scoring CTDNEP1 involvement in lipid droplet biogenesis, cells where automatically threshold and segmented using a Python macro, followed by manual color thresholding and utilization of the Analyze Particles tool in FIJI/ImageJ with 0.9–1.0 particle circularity has the only restriction for LD number.

ER phenotypes were additionally quantified with percent abundance of cytoplasmic calnexin signal. For cells with the entire ER captured within 0.3–0.5 mm interval z stacks, eight-bit maximum intensity projections were made of the whole field of view. To ensure the different ER morphologies were all accounted for after thresholding, the eight-bit max projections were subject to unsharp masking with a radius of two and mask of 0.6. The max intensity projection was thresholded using the Huang threshold of object fuzziness (Huang and Wang, 1995). The cell border and nuclear border for each cell were manually traced using ER fluorescent signal. For percent occupancy of the cytoplasm by ER membranes, the percent of pixels within the nucleus-free cell area that were calnexin (+) was measured.

Statistical analysis

GraphPad Prism 8 was used for all statistical analysis. Continuous data was tested for normality using a Shapiro-Wilk test. In imaging experiments where phenotypes of individual cells are scored, *n* refers to individual cells. All *N* refer to experimental repeats. *p* values, Fisher's exact tests for ER expansion phenotype and One-way Anova with Dunnet's multiple comparisons test for lipid droplet phenotype.

Plasmids or siRNA	Source	Identifier
pcDNA CTDNEP1-HA	(Merta *et al.*, 2021)	
pMRX CTDNEP1-HA	(Merta *et al.*, 2021)	
pMRX CTDNEP1 D67ED69T-HA	(Merta *et al.*, 2021)	
pcDNA CTDNEP1-GFP	(Lee *et al.*, 2023)	
pcDNA AH-EGFP	This study	
pcDNA AH-EGFP 2F2L/A (L10A, F13A, F24A, L28A)	This study	
pcDNA AH-EGFP 3RK/D (R11D, K19D, R29D, R30D)	This study	
pcDNA AH-EGFP 3R/K (R11K, R29K, R30K)	This study	
pcDNA ΔAH-CTDNEP1-EGFP	This study	
pcDNA ΔAH-CTDNEP1-HA	This study	

(*Continues*)

Plasmids or siRNA	Source	Identifier
pMRX ΔAH-CTDNEP1-HA	This study	
pcDNA FLAG-AH-HA	This study	
FLAG-NEP1R1	(Merta *et al.*, 2021)	
pcDNA CTDNEP1-DUB (WT or C23A)-GFP	This study	
pcDNA Nem1(HR)-CTDNEP1-EGFP	This study	
pMRX Nem1(HR)-CTDNEP1-HA	This study	
pcDNA CTDNEP1(V233E)-HA	This study	
pcDNA CTDNEP1(M220AV233A)-HA	This study	
pcDNA FLAG-NEP1R1(F30E)	This study	
pcDNA FLAG-NEP1R1(F30A)	This study	
pMRX CTDNEP1(V233E)-HA	This study	
pcDNA FLAG-mScarlet-NEP1R1	This study	
pcDNA FLAG-mScarlet-NEP1R1 F30E	This study	
pcDNA FLAG-mScarlet-NEP1R1 F30A	This study	
Lamp1-mScarlet	Addgene 98827	
mRFP-Sec61β	DeCamilli lab (Yale University), (Zurek *et al.*, 2011)	
Myc-NEP1R1	This study	
His6-MBP-CTDNEP1ΔAH	This study	
His6-MBP-CTDNEP1ΔAH	This study	
pCMV-VSV-G	(Matsudaira *et al.*, 2017)	N/A
pCG-Gal-Pol	(Matsudaira *et al.*, 2017)	N/A
siNEP1R1 resistant Flag-NEP1R1	This study	
siNEP1R1 resistant Flag-NEP1R1(F30E)	This study	
siRNA targeting sequence: CTDNEP1 smartpool	Dharmacon	Catalogue# M-017869-00-0005
siRNA targeting sequence: Lipin 1 custom single siRNA, no modifications: GAAUGGAAUGCCAGCUGGA	(Sołtysik *et al.*, 2021) Dharmacon	
siRNA targeting sequence: NEP1R1 smartpool	Dharmacon	Catalogue# M-018790-01-0005
Antibodies		
Rabbit α calnexin	Abcam Catalogue#ab22595	AB_2069006
Mouse α GFP	Roche Catalogue#11814460001	AB_390913
Rabbit α calreticulin	Abcam Catalogue#ab2907	AB_303402
Mouse α tubulin DM1A	Millipore Sigma Catalogue#05-829	AB_310035
Mouse α FLAG	Sigma Catalogue#F3165	AB_259529
Mouse α myc	Sigma Catalogue#05-724	N/A
Rabbit α HA	Cell Signalling Technologies Catalogue#3724	AB_1549585
Rabbit α Sun2	Christian Schlieker lab (Yale University; Rose *et al.*, 2014)	N/A
Rabbit α lipin-1	Protein Tech Catalogue#27026-1-AP	AB_2880727
Rabbit α NRF2	Abcam Catalogue#ab62352	AB_944418
Rabbit α LC3B	Novus Catalogue#NB100-2220	AB_10003146
α Ubiquitin HRP	Santa Cruz Catalogue#sc-166553	AB_2241297
Goat α mouse IgG-HRP	Thermo Fisher Catalogue#31430	AB_228307
FITC Goat α mouse	Jackson Immuno Catalogue#115-095-146	AB_2338599
Rhodamine RedX Donkey α rabbit	Jackson Immuno Catalogue#711-295-152	AB_2340613
Goat α rabbit IgG-HRP	Thermo Fisher Catalogue#31460	AB_228341

Chemicals, peptides, and recombinant proteins	Source	Notes
Cycloheximide	Cell Signalling Catalogue#2112	
MG132 z-Leu-Leu-Leu-Al	Fisher Scientific Catalogue#AAJ63250LB0	
CB-5083	ApexBio Catalogue#B6032	
Anti-Flag magnetic beads	Sigma Catalogue#M8823-1 mL	
Anti-HA Magnetic beads	Thermo Fisher Catalogue# PI88836	
3x Flag peptide	ApexBio Catalogue#6001	
Blasticidin	Sigma Catalogue#R21001	
Torin1	ApexBio Catalogue#A8312	
Oleic acid	Cayman Catalogue# 90260	
Bodipy C12 558/568	Thermo Fisher Scientific Catalogue#D3835	
Critical Commercial Assays		
Zymopure II plasmid Midi prep kit	Zymogen Catalogue#D4200	
Pierce BCA Protein Assay kit	Thermo Scientific Catalogue#23225	
Software and Algorithms		
FIJI	(Schindelin *et al*., 2012)	https://imagej.net/Fiji
GraphPad Prism 8/9	GraphPad Software	www.graphpad.com/scientific-software/prism/
AlphaFold	(Jumper *et al*., 2021; Perrakis and Sixma, 2021)	
PyMOL	Schrödinger, LLC	
Image Lab Software	Bio-Rad	www.bio-rad.com/en-us/product/image-lab-software
Cell lines		
U2 OS	(Merta *et al*., 2021)	
U2OS CTDNEP1^EGFP	(Lee *et al*., 2023)	
Cos 7	Bewersdorf lab (Yale University)	
DLD-1 CTDNEP1^mAID-HA	(Lee *et al*., 2023)	
HEK293	Breslow lab (Yale University)	

Oligo name	Sequence	Notes
qPCR Hs CTDNEP1 FWD	CATTTACCTTCTGCGGAGGC	Spans exon 1
qPCR Hs CTDNEP1 REV	CACCTGGGCTAGCCGATTC	Spans exon 2 and 3
qPCR Hs 36B4 FWD	AACATGCTCAACATCTCCCC	
qPCR Hs 36B4 REV	CCGACTCCTCCGACTCTTC	
qPCR Hs NEP1R1 FWD	ccgcgagttgtatccctgat	
qPCR Hs NEP1R1 REV	ccaggcaccagtagctgtac	

ACKNOWLEDGMENTS

We thank M. Hochstrasser, J.M. Gendron, C. Schlieker (Yale University) for helpful discussions; Members of C. Schlieker, J.M. Gendron J. Bewersdorf, D. K. Breslow and P. De Camili (Yale University) laboratories for reagents. Yale Nucleus Club and BMB Club for helpful discussions. This work was supported by: National Institutes of Health (NIH) R01 (GM131004) and National Science Foundation CAREER (1846010) to S.B. Additional support is by NIH (T32 GM722345) to J.W.C.R, Anderson Postdoctoral Fellowship to S.L., and NIH R35 (GM128666) to M.V.A. and the Alfred P. Sloan Foundation to M.V.A.

REFERENCES

Adeyo O, Horn PJ, Lee SK, Binns DD, Chandrahas A, Chapman KD, Goodman JM (2011). The yeast lipin orthologue Pah1p is important for biogenesis of lipid droplets. J Cell Biol 192, 1043–1055.

Bahmanyar S, Biggs R, Schuh AL, Desai A, Muller-Reichert T, Audhya A, Dixon JE, Oegema K (2014). Spatial control of phospholipid flux restricts endoplasmic reticulum sheet formation to allow nuclear envelope breakdown. Genes Dev 28, 121–126.

Baumann O, Walz B (2001). Endoplasmic Reticulum of Animal Cells and Its Organization into Structural and Functional Domains. Int Rev Cytol 205, 149–214.

Christianson JC, Jarosch E, Sommer T (2023). Mechanisms of substrate processing during ER-associated protein degradation. Nat Rev Mol Cell Biol 24, 777–796.

Coleman RA, Lee DP (2004). Enzymes of triacylglycerol synthesis and their regulation. Prog Lipid Res 43, 134–176.
Coleman RAL, Lewin TM, Muoio DM. (2000). Physiological and nutritional regulation of enzymes of triacylglycerol synthesis. Annu Rev Nutr 20, 77–103.
Darrigrand JF, Valente M, Comai G, Martinez P, Petit M, Nishinakamura R, Osorio DS, Renault G, Marchiol C, Ribes V, Cadot B (2020). Dullard-mediated Smad1/5/8 inhibition controls mouse cardiac neural crest cells condensation and outflow tract septation. eLife 9, e50325.
Dey P, Su WM, Mirheydari M, Han GS, Carman GM (2019). Protein kinase C mediates the phosphorylation of the Nem1-Spo7 protein phosphatase complex in yeast. J Biol Chem 294, 15997–16009.
Drin G, Antonny B. (2010). Amphipathic helices and membrane curvature. FEBS Lett 584, 1840–1847.
Fagone P, Jackowski S (2009). Membrane phospholipid synthesis and endoplasmic reticulum function. J Lipid Res 50 (Suppl), S311–S316.
Friedman JR, Lackner LL, West M, DiBenedetto JR, Nunnari J, Voeltz GK (2011). ER Tubules Mark Sites of Mitochondrial Division. Science 334, 358–362.
Gao S, Carrasquillo Rodríguez JW, Bahmanyar S, Airola MV (2024). Structure and mechanism of the human CTDNEP1-NEP1R1 membrane protein phosphatase complex necessary to maintain ER membrane morphology. PNAS 121, e2321167121.
Gautier R, Douguet D, Antonny B, Drin G (2008). HELIQUEST: a web server to screen sequences with specific α-helical properties. Bioinformatics, 24, 2101–2102.
Gimenez-Andres M, Copic A, Antonny B (2018). The Many Faces of Amphipathic Helices. Biomolecules 8, 45.
Goldstein JL, DeBose-Boyd RA, Brown MS (2006). Protein sensors for membrane sterols. Cell 124, 35–46.
Han GS, O'Hara L, Carman GM, Siniossoglou S (2008). An unconventional diacylglycerol kinase that regulates phospholipid synthesis and nuclear membrane growth. J Biol Chem 283, 20433–20442.
Han GS, Wu WI, Carman GM (2006). The Saccharomyces cerevisiae Lipin homolog is a Mg2+-dependent phosphatidate phosphatase enzyme. J Biol Chem 281, 9210–9218.
Han S, Bahmanyar S, Zhang P, Grishin N, Oegema K, Crooke R, Graham M, Reue K, Dixon JE, Goodman JM (2012). Nuclear envelope phosphatase 1-regulatory subunit 1 (formerly TMEM188) is the metazoan Spo7p ortholog and functions in the lipin activation pathway. J Biol Chem 287, 3123–3137.
Harris TE, Huffman TA, Chi A, Shabanowitz J, Hunt DF, Kumar A, Lawrence JC (2007). Insulin controls subcellular localization and multisite phosphorylation of the phosphatidic acid phosphatase, lipin 1. J Biol Chem 282, 277–286.
Huang L-K, Wang M-JJ (1995). Image thresholding by minimizing the measures of fuzzines. Pattern Recognition 28, 41–51.
Jacquemyn J, Foroozandeh J, Vints K, Swerts J, Verstreken P, Gounko NV, Gallego SF, Goodchild R (2021). Torsin and NEP1R1-CTDNEP1 phosphatase affect interphase nuclear pore complex insertion by lipid-dependent and lipid-independent mechanisms. EMBO J 40, e106914.
Jog R, Han GS, Carman GM (2023). Conserved regions of the regulatory subunit Spo7 are required for Nem1–Spo7/Pah1 phosphatase cascade function in yeast lipid synthesis. J Biol Chem 299, 104683–104683.
Jones DT, Jager N, Kool M, Zichner T, Hutter B, Sultan M, Cho YJ, Pugh TJ, Hovestadt V, Stutz AM, *et al.* (2012). Dissecting the genomic complexity underlying medulloblastoma. Nature 488, 100–105.
Jumper J, Evans R, Pritzel A, Green T, Figurnov M, Ronneberger O, Tunyasuvunakool K, Bates R, Zidek A, Potapenko A, *et al.* (2021). Highly accurate protein structure prediction with AlphaFold. Nature 596, 583–589.
Karanasios E, Barbosa AD, Sembongi H, Mari M, Han GS, Reggiori F, Carman GM, Siniossoglou S (2013). Regulation of lipid droplet and membrane biogenesis by the acidic tail of the phosphatidate phosphatase Pah1p. Mol Biol Cell 24, 2124–2133.
Kim Y, Gentry MS, Harris TE, Wiley SE, Lawrence JC, Dixon JE (2007). A conserved phosphatase cascade that regulates nuclear membrane biogenesis. Proc Natl Acad Sci USA 104, 6596–6601.
Krshnan L, Siu WS, Van de Weijer M, Hayward D, Guerrero EN, Gruneberg U, Carvalho P (2022). Regulated degradation of the inner nuclear membrane protein SUN2 maintains nuclear envelope architecture and function. eLife 11, 1–22.
Kwiatek JM, Carman GM (2020). Yeast phosphatidic acid phosphatase Pah1 hops and scoots along the membrane phospholipid bilayer. J Lipid Res 61, 1232–1243.
Kwiatek JM, Han GS, Carman GM (2020). Phosphatidate-mediated regulation of lipid synthesis at the nuclear/endoplasmic reticulum membrane. Biochim Biophys Acta Mol Cell Biol Lipids 1865, 158434–158434.
Lee S, Carrasquillo Rodríguez JW, Merta H, Bahmanyar S (2023). A membrane-sensing mechanism links lipid metabolism to protein degradation at the nuclear envelope. J Cell Biol 222. e202304026.
Luo Z, Xin D, Liao Y, Berry K, Ogurek S, Zhang F, Zhang L, Zhao C, Rao R, Dong X, *et al.* (2023). Loss of phosphatase CTDNEP1 potentiates aggressive medulloblastoma by triggering MYC amplification and genomic instability. Nat commun 14, 762–762.
Matsudaira T, Mukai K, Noguchi T, Hasegawa J, Hatta T, Iemura SI, Natsume T, Miyamura N, Nishina H, Nakayama J, *et al.* (2017). Endosomal phosphatidylserine is critical for the YAP signalling pathway in proliferating cells. Nat Commun 8, 1246.
Mehrtash AB, Hochstrasser M (2018). Ubiquitin-dependent protein degradation at the endoplasmic reticulum and nuclear envelope. Semin Cell Dev Biol 93, 111–124.
Merta H, Carrasquillo Rodríguez JW, Anjur-Dietrich MI, Vitale T, Granade ME, Harris TE, Needleman DJ, Bahmanyar S (2021). Cell cycle regulation of ER membrane biogenesis protects against chromosome missegregation. Dev Cell 56, 3364–3379.e3310.
Meyer H, Bug M, Bremer S (2012). Emerging functions of the VCP/p97 AAA-ATPase in the ubiquitin system. Nat Cell Biol 14, 117–123.
Mirheydari M, Dey P, Stukey GJ, Park Y, Han GS, Carman GM (2020). The Spo7 sequence LLI is required for Nem1-Spo7/Pah1 phosphatase cascade function in yeast lipid metabolism. J Biol Chem 295, 11473–11485.
O'Hara L, Han GS, Peak-Chew S, Grimsey N, Carman GM, Siniossoglou S (2006). Control of phospholipid synthesis by phosphorylation of the yeast lipin Pah1p/Smp2p Mg2+-dependent phosphatidate phosphatase. J Biol Chem 281, 34537–34548.
Olzmann JA, Carvalho P (2019). Dynamics and functions of lipid droplets. Nat Rev Mol Cell Biol 20, 137–155.
Papagiannidis D, Bircham PW, Lüchtenborg C, Pajonk O, Ruffini G, Brügger B, Schuck S (2021). Ice2 promotes ER membrane biogenesis in yeast by inhibiting the conserved lipin phosphatase complex. EMBO J 40, e107958.
Park Y, Han GS, Carman GM (2017). A conserved tryptophan within the WRDPLVDID domain of yeast Pah1 phosphatidate phosphatase is required for its in vivo function in lipid metabolism. J Biol Chem 292, 19580–19589.
Penfield L, Shankar R, Szentgyorgyi E, Laffitte A, Mauro MS, Audhya A, Muller-Reichert T, Bahmanyar S (2020). Regulated lipid synthesis and LEM2/CHMP7 jointly control nuclear envelope closure. J Cell Biol 219, e201908179.
Perrakis A, Sixma TK (2021). AI revolutions in biology: The joys and perils of AlphaFold. EMBO Rep 22, e54046.
Peterson TR, Sengupta SS, Harris TE, Carmack AE, Kang SA, Balderas E, Guertin DA, Madden KL, Carpenter AE, Finck BN, Sabatini DM (2011). MTOR complex 1 regulates lipin 1 localization to control the srebp pathway. Cell 146, 408–420.
Reue K (2009). The lipin family: mutations and metabolism. Curr Opin Lipidol 20, 165–170.
Rose AE, Zhao C, Turner EM, Steyer AM, Schlieker C (2014). Arresting a Torsin ATPase reshapes the endoplasmic reticulum. J Biol Chem 289, 552–564.
Rose CM, Isasa M, Ordureau A, Prado MA, Beausoleil SA, Jedrychowski MP, Finley DJ, Harper JW, Gygi SP (2016). Highly Multiplexed Quantitative Mass Spectrometry Analysis of Ubiquitylomes. Cell Syst 3, 395–403.e394.
Saik NO, Ptak C, Rehman S, Aitchison JD, Montpetit B, Wozniak RW (2023). SUMOylation at the inner nuclear membrane facilitates nuclear envelope biogenesis during mitosis. J Cell Biol 222, e202208137.
Sakaguchi M, Sharmin S, Taguchi A, Ohmori T, Fujimura S, Abe T, Kiyonari H, Komatsu Y, Mishina Y, Asashima M, *et al.* (2013). The phosphatase Dullard negatively regulates BMP signaling and is essential for nephron maintenance after birth. Nat Commun 4, 1398.
Santos-Rosa H, Leung J, Grimsey N, Peak-Chew S, Siniossoglou S (2005). The yeast lipin Smp2 couples phospholipid biosynthesis to nuclear membrane growth. EMBO J 24, 1931–1941.
Satow R, Kurisaki A, Chan TC, Hamazaki TS, Asashima M (2006). Dullard promotes degradation and dephosphorylation of BMP receptors and is required for neural induction. Dev Cell 11, 763–774.
Schindelin J, Arganda-Carreras I, Frise E, Kaynig V, Longair M, Pietzsch T, Preibisch S, Rueden C, Saalfeld S, Schmid B, *et al.* (2012). Fiji: an open-source platform for biological-image analysis. Nat Methods 9, 676–682.
Schlieker C, Weihofen WA, Frijns E, Kattenhorn LM, Gaudet R, Ploegh HL (2007). Structure of a herpesvirus-encoded cysteine protease reveals a unique class of deubiquitinating enzymes. Mol Cell 25, 677–687.

Seifried A, Schultz J, Gohla A (2013). Human HAD phosphatases: structure, mechanism, and roles in health and disease. FEBS J 280, 549–571.
Siniossoglou S, Santos-Rosa H, Rappsilber J, Mann M, Hurt E (1998). A novel complex of membrane proteins required for formation of a spherical nucleus. EMBO J 17, 6449–6464.
Sołtysik K, Ohsaki Y, Tatematsu T, Cheng J, Maeda A, Morita SY, Fujimoto T (2021). Nuclear lipid droplets form in the inner nuclear membrane in a seipin-independent manner. Jcell biol 220, e202005026.
Stevenson J, Huang EY, Olzmann JA (2016). Endoplasmic Reticulum-Associated Degradation and Lipid Homeostasis. Annu Rev Nutr 36, 511–542.
Su WM, Han GS, Dey P, Carman GM (2018). Protein kinase A phosphorylates the Nem1-Spo7 protein phosphatase complex that regulates the phosphorylation state of the phosphatidate phosphatase Pah1 in yeast. J Biol Chem 293, 15801–15814.
Tsai PL, Zhao C, Turner E, Schlieker C (2016). The Lamin B receptor is essential for cholesterol synthesis and perturbed by disease-causing mutations. eLife 5, e16011.
Walther TC, Farese RV, Jr. (2012). Lipid droplets and cellular lipid metabolism. Annu Rev Biochem 81, 687–714.
Zurek N, Sparks L, Voeltz G (2011). Reticulon short hairpin transmembrane domains are used to shape ER tubules. Traffic 12, 28–41.